Isotope Geology

Part I: Radiometric Geochronology

Pieter Vermeesch
London Geochronology Centre
University College London

p.vermeesch@ucl.ac.uk
+44 (0)20 3108 6369
KLB 116

doi:10.17605/OSF.IO/SJ4FT

Contents

Chapter 1

Introduction

The field of *Isotope Geology* investigates the isotopic composition of major and trace elements contained in rocks and minerals, with the aim to better understand geological processes. Isotopic techniques are used to address a wide range of geological problems, such as the age of the Earth, the origin and formation of magmatic rocks, palaeotemperatures in sedimentary basins, palaeoclimatology etc. Isotope geochemistry forms an integral part of modern Earth Sciences and numerous important discoveries have been made thanks to this research. Every Earth Scientist needs to be aware of these techniques in order to understand research reports and geological intepretations based on isotopic methods. Isotope geochemistry plays an important role in peripheral fields of research such as planetology (origin and evolution of the Solar system) and archaeology (origin and age of settlements, tools and artifacts).

The use of naturally occurring radioactive isotopes to date minerals and rocks is the oldest and best known branch of isotope geology. The foundations of these so-called isotopic or radiometric dating methods were laid shortly after the turn of the XX$^{\text{th}}$ century with the discovery of the laws of radioactive decay by eminent physicists such as Ernest Rutherford and Frederick Soddy (Rutherford and Soddy, 1902a,b). The application of these principles to the field of Geology and the calibration of the geological time scale were pioneered by Arthur Holmes (1911, 1913, 1947). Initially, radiometric geochronology was exclusively based on uranium and its daughter products, but with the

development of increasingly sensitive analytical equipment, ever more isotopic 'clocks' were added over the course of the century: Rb/Sr (Hahn et al., 1943), ^{14}C (Libby, 1946), K/Ar (Aldrich and Nier, 1948), ^{238}U fission tracks (Price and Walker, 1963), ^{40}Ar/^{39}Ar (Merrihue and Turner, 1966), Sm/Nd (Lugmair, 1974), etc.

During the 1960s, geochemists began to investigate the isotopic composition of elements which are partly made of radiogenic isotopes with the aim to understand the source and origin of the igneous rocks. This line of research greatly expanded over the course of the 1970s and 80s and nowadays the isotopic composition of elements such as Sr and Nd in rocks and minerals is generally considered as an important petrogenetic indicator. The discovery that the isotopes of the light elements (H, C, N, O, S) are fractionated by physical and chemical processes dates back to the 1930s. The isotopic composition of these elements can therefore be used to detect and understand the hydrospheric and lithospheric processes causing such fractionation (Urey, 1947). This has led to a better understanding of the physiochemical conditions under which rocks and minerals are formed. Temperature is the most important of these conditions and the aforementioned elements are often used for palaeothermometry.

These lecture notes cover the first half of an Isotope Geology module at UCL that deals with the geochronological aspects of the subject. The second part of the module deals with stable isotopes. It is taught by Dr. Philip Pogge Von Strandmann and covered in a separate set of notes. The core of the geochronology notes is formed by Prof. Peter van den Haute's lecture notes (in Dutch) at the University of Ghent. This was expanded with additional material, notably on the subjects of cosmogenic nuclide geochronology (Section 8) and U-Th-He dating (Section 7.1). Some figures were modified from published sources, including Allègre (2008), Braun et al. (2006), and Galbraith (2005). These books are recommended further reading material, as is the detailed textbook by Dickin (2005), from which both Prof. van den Haute's notes and Allègre (2008) heavily borrow. Additional lecture material, including the data files used in the `Matlab` practicals of Section 12, can be found at `http://github.com/pvermees/geotopes`.

Bibliography

Aldrich, L. T. and Nier, A. O. Argon 40 in potassium minerals. *Physical Review*, 74(8):876, 1948.

Allègre, C. J. *Isotope geology*. Cambridge University Press, 2008.

Braun, J., Van Der Beek, P., and Batt, G. *Quantitative thermochronology: numerical methods for the interpretation of thermochronological data*. Cambridge University Press, 2006.

Dickin, A. P. *Radiogenic isotope geology*. Cambridge University Press, 2005.

Galbraith, R. F. *Statistics for fission track analysis*. CRC Press, 2005.

Hahn, O., Strassman, F., Mattauch, J., and Ewald, H. Geologische Altersbestimmungen mit der strontiummethode. *Chem. Zeitung*, 67: 55–6, 1943.

Holmes, A. The association of lead with uranium in rock-minerals, and its application to the measurement of geological time. *Proceedings of the Royal Society of London. Series A, Containing Papers of a Mathematical and Physical Character*, 85(578):248–256, 1911.

Holmes, A. *The age of the Earth*. Harper & Brothers, 1913.

Holmes, A. The Construction of a Geological Time-Scale. *Transactions of the Geological Society of Glasgow*, 21(1):117–152, 1947.

Libby, W. F. Atmospheric helium three and radiocarbon from cosmic radiation. *Physical Review*, 69(11-12):671, 1946.

Lugmair, G. Sm-nd ages: a new dating method. *Meteoritics*, 9:369, 1974.

Merrihue, C. and Turner, G. Potassium-argon dating by activation with fast neutrons. *Journal of Geophysical Research*, 71(11):2852–2857, 1966.

Price, P. and Walker, R. Fossil tracks of charged particles in mica and the age of minerals. *Journal of Geophysical Research*, 68(16): 4847–4862, 1963.

Rutherford, E. and Soddy, F. The cause and nature of radioactivity – part i. *The London, Edinburgh, and Dublin Philosophical Magazine and Journal of Science*, 4(21):370–396, 1902a.

Rutherford, E. and Soddy, F. The cause and nature of radioactivity – part ii. *The London, Edinburgh, and Dublin Philosophical Magazine and Journal of Science*, 4(23):569–585, 1902b.

Urey, H. C. The thermodynamic properties of isotopic substances. *Journal of the Chemical Society (Resumed)*, pages 562–581, 1947.

Chapter 2

Basic notions of radiometric geochronology

2.1 Isotopes and radioactivity

Thanks to discoveries by Niels Bohr, Ernest Rutherford, Arnold Sommerfeld, Joseph Thomson and James Chadwick, we know that rocks and minerals are made of atoms, atoms are made of a nucleus and an electron cloud, and the nucleus is made of *nucleons* of which there are two kinds: protons and neutrons. The total number of nucleons in the atomic nucleus is called the *mass number* (A). The number of protons (which equals the number of electrons in a neutral atom) is called the *atomic number* (Z). The chemical properties of a nuclide solely depend on the atomic number, which therefore forms the basis of the Periodic Table of Elements. The number of neutrons in the atomic nucleus may take on a range of values for any given element, corresponding to different *isotopes* of said element. For example, $^{16}_{8}$O is an isotope of oxygen with 16 nucleons of which 8 are protons (and N = A-Z = 16-8 = 8 are neutrons). Adding one extra neutron to the nucleus produces a second oxygen isotope, $^{17}_{8}$O, with identical chemical properties as $^{16}_{8}$O, but slightly different physical properties (e.g. boiling temperature). Adding another neutron produces $^{18}_{8}$O which, with 8 protons and 10 neutrons, is more than 10% heavier than $^{16}_{8}$O. Due to this mass

difference, the $^{18}_{8}O/^{16}_{8}O$ ratio undergoes *mass fractionation* by several natural processes, forming the basis of $^{18}_{8}O/^{16}_{8}O$ palaeothermometry (see the second half of this course). When we try to add yet another neutron to the atomic nucleus of oxygen, the nucleus becomes unstable and undergoes radioactive decay. Therefore, no $^{19}_{8}O$ exists in Nature.

2.2 Radioactivity

As mentioned before, the Periodic Table of Elements (aka 'Mendeleev's Table') arranges the elements according to the atomic number and the configuration of the electron cloud. The equally important *Chart of Nuclides* uses both the number of protons and neutrons as row and column indices. At low masses, the stable nuclides are found close to the $1 \div 1$ line ($N \approx Z$), with the radionuclides found at higher and lower ratios. At higher atomic numbers, the stable nuclides are found at higher mass numbers, reflecting the fact that more neutrons are required to keep the protons together. For example, $^{208}_{82}Pb$, which is the heaviest stable nuclide, has 44 more neutrons than protons. The unstable nuclides (or *radionuclides*), such as $^{209}_{82}Pb$ or $^{19}_{8}O$ may survive for time periods of femtoseconds to billions of years depending on the degree of instability, which generally scales with the 'distance' from the curve of stable nuclides. Radionuclides eventually disintegrate to a stable form by means of a number of different mechanisms:

1. α-decay
   The atomic nucleus (e.g., $^{238}_{92}U$, $^{235}_{92}U$, $^{232}_{90}Th$, $^{147}_{62}Sm$) loses an α particle, i.e. the equivalent of a $^{4}_{2}He$ nucleus. When these nuclei acquire electrons, they turn into Helium atoms, forming the basis of the U-Th-He chronometer, which is further discussed in Section 7.1. The recoil energy of the decay is divided between the α particle and the parent nucleus, which eventually relaxes into its ground state by emitting γ radiation, i.e. photons with a wavelength of 10^{-10}m or less. In addition to the aforementioned U-Th-He method, α-decay is central to the ^{147}Sm-^{143}Nd (Section 4.2), ^{235}U-^{207}Pb, ^{238}U-^{206}Pb and ^{232}Th-^{208}Pb methods (Section 5).

2. β-decay
   Comprises negatron (β^-) and positron (β^+) emission, in which either an electron or a positron is emitted from the nucleus, causing a transition of (N,Z) $\rightarrow$ (N-1,Z+1) for β^- decay and (N,Z)

$\rightarrow$ (N+1,Z-1) for β^+ decay. For example, the oxygen isotope $^{19}_{8}$O discussed in Section 2.1 decays to $^{19}_{9}$F by β^- emission. In contrast with α particles, which are characterized by discrete energy levels, β particles are characterised by a continuous energy spectrum. The difference between the maximum kinetic energy and the actual kinetic energy of any given emitted electron or positron is carried by a neutrino (for β^+ decay) or an anti-neutrino (for β^- decay). Just like α decay, β decay is also accompanied by γ-radiation, arising from two sources: (a) relaxation into the ground state of the excited parent nucleus and (b) spontaneous annihilation of the unstable positron in β^+ decay. β^- decay is important for the ^{40}K-^{40}Ca, ^{87}Rb-^{87}Sr (Section 4.2) and ^{14}C-^{14}N (Section 4.1) clocks. It also occurs as part of the ^{235}U-^{207}Pb, ^{238}U-^{206}Pb and ^{232}Th-^{208}Pb decay series (Sections 5 and 9). β^+ decay is found in the ^{40}K-^{40}Ar system (Section 6).

3. electron capture
This is a special form of decay in which an 'extra-nuclear' electron (generally from the K-shell) is captured by the nucleus. This causes a transformation of (N,Z) $\rightarrow$ (N+1,Z-1), similar to positron emission, with which if often co-exists. The vacant electon position in the K-shell is filled with an electron from a higher shell, releasing X-rays ($\sim 10^{-10}$m wavelength), which is the diagonistic signal of electron capture. This mechanism occurs in the ^{40}K-^{40}Ar decay scheme (Section 6).

4. nuclear fission
Extremely large nuclei may disintegrate into two daughter nuclei of unequal size, releasing large amounts of energy ($\sim$ 200 MeV). The two daughter nuclei move in opposite directions from the parent location, damaging the crystal lattice of the host mineral in their wake. The two daughter nuclides are generally radioactive themselves, giving rise to β radiation before coming to rest as stable isotopes. $^{238}_{92}$U is the only naturally occurring nuclide which undergoes this type of radioactive decay in measurable quantities, and even then it only occurs once for every $\sim 2\times10^6$ α decay events. Nevertheless, the fission mechanism forms the basis of an important geochronological method, in which the damage zones or 'fission tracks' are counted (Section 7.2). Nuclear fission can also be artificially induced, by neutron irradiation of ^{235}U, e.g.:

$$^{235}_{92}\mathrm{U} + \mathrm{n} \rightarrow {}^{236}_{92}\mathrm{U} \rightarrow {}^{90}_{36}\mathrm{Kr} + {}^{143}_{56}\mathrm{Ba} + 3\mathrm{n} + \text{energy} \qquad (2.1)$$

Note that every neutron on the left hand side of this formula generates three neutrons on the right hand side. The latter may react with further ^{235}U nuclei and generate a chain reaction which forms the basis of nuclear reactors, the atom bomb and the 'external detector' method (Section 7.2).

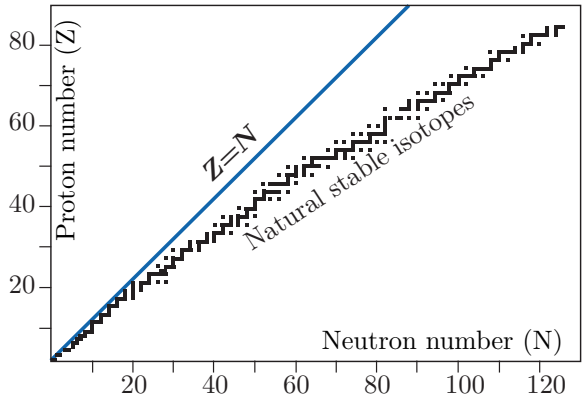

Figure 2.1: A schematic '*Chart of Nuclides*' (modified from Allègre, 2008).

2.3 The age equation

A characteristic property of radioactive decay is its absolute independence of external physical and chemical effects. In other words, it is not affected by changes in pressure, temperature, or the molecular bonds connecting a radioactive nuclide to neighbouring atoms. This means that the rate at which a radioactive parent atom (P) decays to a radiogenic daughter (D) per unit time, i.e. dN_P/dt only depends on N_P, the number of parent atoms present. The *decay constant* λ expresses the likelihood that a radioactive disintegration takes place in any given time (i.e., λ has units of atoms per atoms per year). This can be expressed mathematically with the following differential equation:

$$\frac{dN_P}{dt} = -\lambda N_P \tag{2.2}$$

Integrating this equation over time yields:

$$N_P = (N_P)_\circ e^{-\lambda t} \tag{2.3}$$

where $(N_P)_\circ$ is the number of parent atoms present at time $t = 0$. Since this number is generally unknown (one exception is ^{14}C, see Section 4.1), Equation 2.3 generally cannot be used in this form. We can, however, measure the *present* number of parent and daughter nuclides in the sample. Rewriting Equation 2.3:

$$(N_P)_\circ = N_P e^{\lambda t} \tag{2.4}$$

and bearing in mind that $N_D = (N_P)_\circ - N_P$, we obtain:

$$N_D = N_P(e^{\lambda t} - 1) \tag{2.5}$$

This equation forms the foundation of most geochronological methods. It can be rewritten explicitly as a function of time:

$$t = \frac{1}{\lambda} \ln\left(\frac{N_D}{N_P} + 1\right) \tag{2.6}$$

The degree of instability of a radioactive nuclide can be expressed by λ or by the *half life* $t_{1/2}$, which is the time required for half of the parent nuclides to decay. This follows directly from Equation 2.3:

$$\frac{(N_P)_\circ}{2} = (N_P)_\circ e^{-\lambda t_{1/2}} \Rightarrow t_{1/2} = \frac{\ln(2)}{\lambda} \tag{2.7}$$

As a rule of thumb, the detection limit of a radiometric geochronometer is reached after about 10 half lives. Thus, ^{14}C goes back ∼50,000 years, ^{10}Be 10 million and ^{40}K 10 billion years.

2.4 Decay series

Sometimes the radiogenic daughter (D_1) of a radioactive parent is radioactive as well, decaying to a daughter of its own (D_2), which may be radioactive again etc., until a stable daughter (D_*) is reached. Considering the simplest case of one intermediate daughter:

$$P \xrightarrow{\lambda_P} D_1 \xrightarrow{\lambda_1} D_* \tag{2.8}$$

The increase (or decrease) of the number of atoms per unit time for each of the nuclides is given by:

$$\text{for } P : dN_P/dt = -\lambda_P N_P \tag{2.9}$$
$$\text{for } D_1 : dN_{D_1}/dt = \lambda_P N_P - \lambda_1 N_{D_1} \tag{2.10}$$
$$\text{for } D_* : dN_{D_*}/dt = -\lambda_1 N_{D_1} \tag{2.11}$$

The number of atoms N_P can be written as a function of t:

$$N_P = (N_P)_\circ e^{-\lambda_P t} \tag{2.12}$$

Plugging Equation 2.12 into 2.10 yields

$$dN_{D_1}/dt = \lambda_P (N_P)_\circ e^{-\lambda_P t} - \lambda_1 N_{D_1} \tag{2.13}$$

Solving this differential equation yields the evolution of D_1 with time. Assuming that $N_{D_1} = 0$ at $t = 0$:

$$N_{D_1} = \frac{\lambda_P}{\lambda_1 - \lambda_P}(N_P)_\circ \left[e^{-\lambda_P t} - e^{-\lambda_1 t}\right] \tag{2.14}$$

If $\lambda_P \ll \lambda_1$ (by a factor of 10 or greater), then $e^{-\lambda_1 t}$ becomes vanishingly small relative to $e^{-\lambda_P t}$ after a sufficiently long time so that Equation 2.14 can be simplified:

$$N_{D_1} = \frac{\lambda_P}{\lambda_1 - \lambda_P}(N_P)_\circ e^{-\lambda_P t} \tag{2.15}$$

or, alternatively:

$$N_{D_1} = \frac{\lambda_P}{\lambda_1 - \lambda_P} N_P \tag{2.16}$$

This means that the ratio of N_{D_1} and N_P remains constant through time. If $\lambda_P \ll \lambda_1$, then $\lambda_1 - \lambda_P \approx \lambda_1$, from which it follows that:

$$N_{D_1} = \frac{\lambda_P}{\lambda_1} N_P \tag{2.17}$$

Rearranging:

$$N_{D_1}\lambda_1 = N_P \lambda_P \tag{2.18}$$

or, equivalently:

$$\frac{N_P}{N_{D_1}} = \frac{t_{1/2}(P)}{t_{1/2}(D_1)} \tag{2.19}$$

This is the *secular equilibrium* in which the number of atoms of both radioactive members is proportional to their respective half lives. In the geochronological isotope systems $^{235}U/^{207}Pb$, $^{238}U/^{206}Pb$ and $^{232}Th/^{207}Pb$, the lead isotopes are the end points of a long decay series comprised of several α and β^- disentegrations, in which the decay constants of the parent nuclide is orders of magnitude shorter than the other nuclides in the chain. For a decay series like that, Equation 2.18 can be generalised to:

$$N_{D_n}\lambda_n = \cdots = N_{D_2}\lambda_2 = N_{D_1}\lambda_1 = N_P\lambda_P \tag{2.20}$$

This means that the entire series is in equilibrium, so that all members occur in mutually constant proportions. The number of atoms of the stable end member D_* is given by:

$$N_{D_*} = (N_P)_\circ - N_P - N_{D_1} - N_{D_2} - \cdots N_{D_n} \tag{2.21}$$

Using Equation 2.20, this becomes:

$$N_{D_*} = (N_P)_\circ - N_P - \frac{N_P\lambda_P}{\lambda_1} - \frac{N_P\lambda_P}{\lambda_2} - \cdots - \frac{N_P\lambda_P}{\lambda_n} \tag{2.22}$$

or

$$N_{D_*} = (N_P)_\circ - N_P\left(1 + \frac{\lambda_P}{\lambda_1} - \frac{\lambda_P}{\lambda_2} - \cdots - \frac{\lambda_P}{\lambda_n}\right) \tag{2.23}$$

Since each of the ratios λ_P/λ_1, λ_P/λ_2, etc. are vanishingly small, we can simplify Equation 2.23 as:

$$N_{D_*} = (N_P)_\circ - N_P = N_P\left(e^{\lambda_P t} - 1\right) \tag{2.24}$$

This means that the accumulation of the final Pb isotope of the aforementioned three decay series is only a function of the decay of the parent isotope. All intermediate decay steps are therefore inconsequential. In rare cases, however, the isotopic equilibrium is disturbed by a dissolution or recrystallisation event, say. The intermediate parent/daughter pairs can then be used to date phenomena occuring over

much shorter time scales than those probed by the U-Pb method (Section 9).

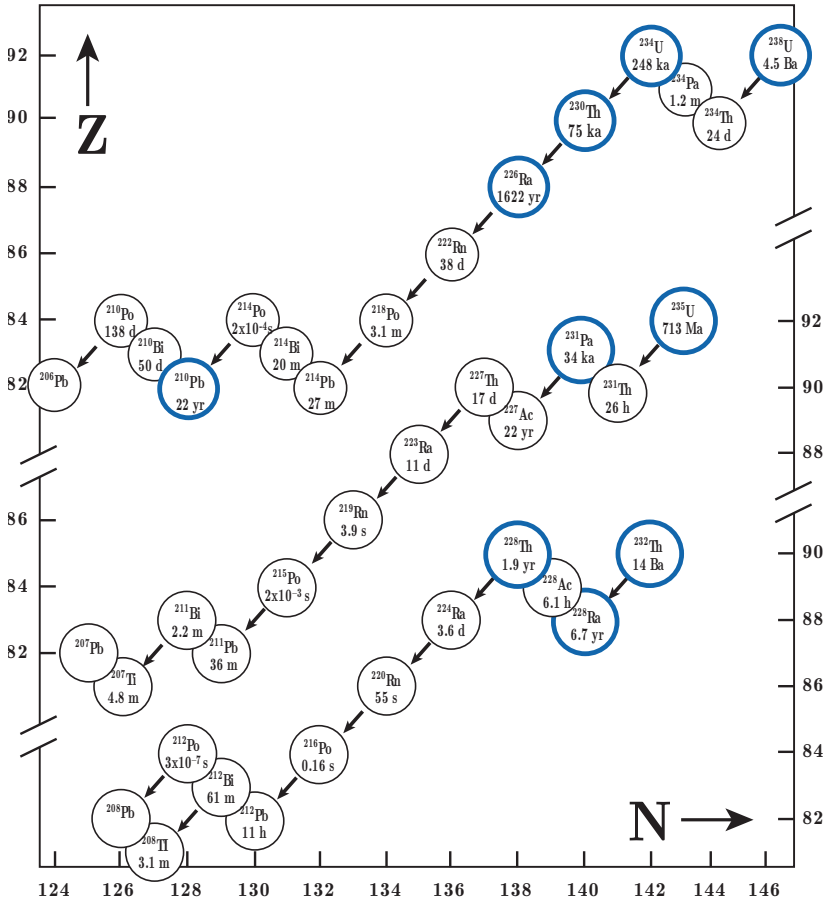

Figure 2.2: The decay series of ^{232}Th, ^{235}U and ^{238}U, which form the basis of the U-Th-Pb, U-Th-He and U-Th-series methods (modified from Allègre, 2008).

Chapter 3

Analytical techniques

Isotope geochemistry is based on the accurate and precise determination of elemental and isotopic compositions of rocks and minerals. Although some of the earliest geochronological methods (notably the ^{14}C method, see Section 4.1) were based on the detection of radioactivity by means of Geiger-Müller counters and liquid scintillation detectors, nearly all modern isotope geochemistry is done by mass spectrometry.

3.1 Mass spectrometry

A mass spectrometer is a device that separates electrically charged atoms or molecules based on their mass, enabling precise measurement of the isotopic composition. A mass spectrometer consists of the following parts:

1. ion source: this can be either a filament (similar to that found in an incandescent light bulb), a plasma torch, a primary ion beam, or a spray chamber, among other possibilities.

2. mass analyser: this can be an electromagnet (possibly combined with an electrostatic field), or a rapidly fluctuationg electric field.

3. ion detector: this is, essentially, a volt meter.

In the remainder of this section, we will assume the source to be a filament and the mass analyser to be an electromagnet.

After pumping the mass spectrometer down to (ultra-)high vacuum conditions (10^{-6} to 10^{-9} mbar), the sample enters the ion source as a gas, where it is bombarded with electrons. The resulting ions (with charge e) are accelerated in an electric field (with potential difference V) and collimated to a narrow beam. This beam is sent through a magnetic field (with strength H) which deflects it into a circular trajectory with a radius proportional to the ion mass (m). This results in a physical separation of the incoming ion beam into various outgoing beams. The beams of interest are steered into the ion detector which, in its simplest design (the so-called 'Faraday Cup') consists of a long and narrow cup. The ion beam is neutralised in the cup by electrons flowing from ground through a resistor. The potential difference across this resistor is measured and registered on a computer for further processing.

The electric field transfers a certain amount of kinetic energy to the ions:

$$E = eV = \frac{mv^2}{2} \tag{3.1}$$

With e is the electrical charge (in multiples of 1.60219 $\times 10^{-19}$C, which is the elementary charge of an electron. Because each type of ion has a different mass (m, in multiples of 1.660538 $\times 10^{-27}$kg, the atomic mass unit), their terminal velocity (v) differs as well:

$$v = \sqrt{\frac{2eV}{m}} \tag{3.2}$$

The mass analyser deflects the ions according to the following equation:

$$Hev = \frac{mv^2}{r} \tag{3.3}$$

Substituting Equation 3.2 into 3.3 yields:

$$H\sqrt{\frac{2eV}{m}} = \frac{2V}{r} \tag{3.4}$$

from which it follows that:

$$r = \frac{1}{H}\sqrt{\frac{2mV}{e}} \qquad \textit{and} \qquad H = \frac{1}{r}\sqrt{\frac{2mV}{e}} \tag{3.5}$$

Equation 3.5 allows us to calculate the radius of the ion trajectory for any given mass-to-charge ratio m/e. Note that light isotopes are more strongly deflected than equally charged heavy ones. Equation 3.5 can also be used to calculate the magnetic field strength required to deflect an ion beam with a given m/e ratio into the collector. This is more practical because most mass spectrometers have a fixed radius so that the different ions must be collected by varying H. Some modern mass spectrometers are equipped with multiple ion collectors the enabling simultaneous analysis of several ionic masses.

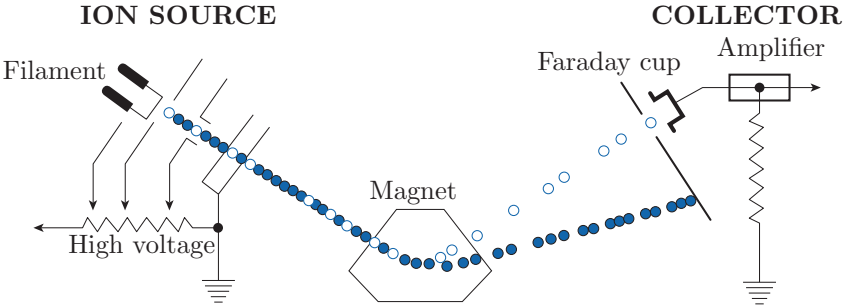

Figure 3.1: Schematic diagram of a sector-field noble gas or TIMS mass spectrometer (modified from Allègre, 2008).

Several types of mass spectrometers are used for geoscience applications:

1. *Thermal Ionisation Mass Spectrometry (TIMS).*
   The sample is dissolved and subjected to careful chemical separation procedures (liquid chromatography) in order to separate the parent and daughter elements to a high level of purity. The resulting solutions are spiked and deposited on a tungsten or tantalum filament, which is brought to a glow by an electric current and thus produces ions. These are separated by a large electromagnet and analysed in one or more Faraday cups. TIMS is very time consuming but produces extremely precise results (‰-level precision on the ages).

2. *Inductively Coupled Plasma Mass Spectrometry (ICP-MS).*
The sample is vapourised in one of two ways: either by introducing a liquid into a spray chamber, or by firing an ultraviolet laser at a solid sample and transporting the resulting aerosol into the ion source with a carrier gas (typically helium). The ion source itself consists of an argon flow which is heated to a temperature of approximately 10,000K by sending a radiofrequency current through a coil. This breaks up all the molecular bonds and produces a plasma (i.e. a 'soup' of ions and electrons) which enters the high vacuum chamber through a tiny opening. The mass analyser can either be a sector magnet or a quadrupole (which consists of four metal rods generating a rapidly fluctuating electrical field). ICP-MS offers a higher throughput than TIMS, especially in laser ablation mode, where hundreds of ages can be measured per day. However, this increased throughput comes at the expense of precision, which is on the percent level (better in solution mode).

3. *Secondary ion mass spectrometry (SIMS)*
Prior to the develoment of laser ablation (LA-) ICP-MS, the only other method to produce spot measurements in solid samples was by firing a beam of negative (e.g. oxygen) or positive (e.g. caesium) ions at the target under high vacuum. This releases ('sputters') positive (or negative, in the case of a Cs beam) *secondary* ions from the sample surface, which are accelerated by an electrostatic field and sent to a sector field mass spectrometer. Although SIMS has been replaced by LA-ICP-MS in some applications, it remains an important instrument in the geochronological toolbox because (a) it offers higher spatial resolution than laser ablation (5-10μm vs. 25-50μm) and (b) can measure light ions (e.g, hydrogen) more reliably than LA-ICP-MS.

4. *Accelerator Mass Spectrometer (AMS)*
The AMS combines two mass spectrometers with a ('tandem' type) particle accelerator. Ions are produced by a SIMS source and steered through a first mass analyser, which selects all ions of a desired mass (e.g., mass 14: $^{14}C^-$, $^{12}CH_2^-$, $\cdots$). The resulting beam is accelerated in the first part of the tandem accelerator by a potential difference of several million eV, and sent through a thin chamber filled with a 'stripper' gas. Collisions of stripper gas atoms with the incoming ions destroys any molecular bonds

and forms 3+ ions in the process. The beam now consists of purely atomic ions, which are accelerated in the second part of the accelerator and steered into a second mass analyser. The AMS has revolutionised the ^{14}C method by enabling the analysis of extremely small (mg-sized) samples (see Section 4.1), and has enabled a whole new field of geochronology based on the analysis of terrestrial cosmogenic radionuclides (Chapter 8). The main limitation of AMS is its high cost. Currently only two AMS facilities are operating in the UK (in Oxford and Glasgow).

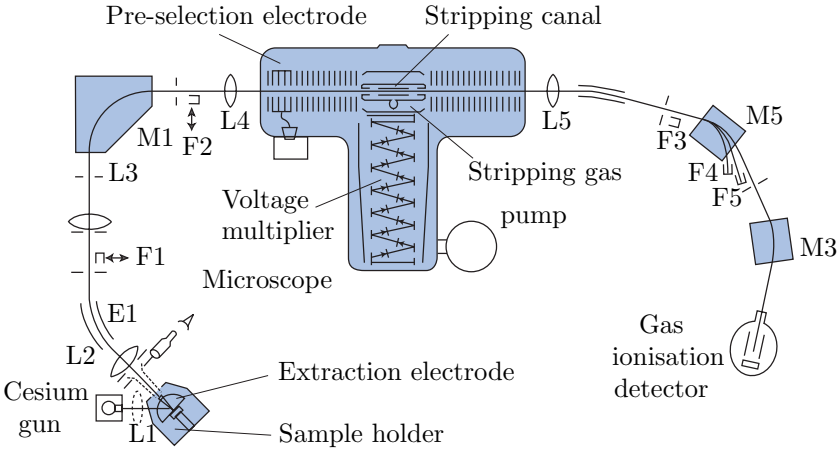

Figure 3.2: Schematic diagram of an Accelerator Mass Spectrometer (AMS) (modified from Allègre, 2008).

3.2 Isotope dilution

Besides determining isotopic compositions, the mass spectrometer can also be used to measure elemental concentrations, using a method called *isotope dilution*. This is done by mixing the sample solution (whose isotopic composition has already been determined) with a known quantity of a solution with a different (but known) isotopic composition and known elemental concentration. The latter solution is called the *spike*. The isotopic composition of the mixture is analysed by mass spectrometry. The measured isotopic ratio R_m for an element with two isotopes (^aX and ^bX) is given by:

$$R_m = \frac{N\,{}^aX_N + S\,{}^aX_S}{N\,{}^bX_N + S\,{}^bX_S} \tag{3.6}$$

with

$N =$ the number of atoms of X in the sample
$S =$ the number of atoms of X in the spike
${}^aX_N, {}^bX_N =$ the atomic abundance of isotope a (or b) in the
${}^aX_S, {}^bX_S$ sample (or spike)$({}^aX_N + {}^bX_N = {}^aX_S + {}^bX_S = 1)$

N is the only unknown in Equation 3.6, which can therefore be rewritten as:

$$N = S\frac{{}^aX_S - R_m\,{}^bX_S}{R_m\,{}^bX_N - {}^aX_N} \tag{3.7}$$

N can also be expressed as a function of the isotopic ratios in the sample $R_N(= {}^aX_N/{}^bX_N)$ and in the spike $R_S(= {}^aX_S/{}^bX_S)$. The atomic abundance of ${}^aX$ and ${}^bX$ in the sample are given by:

$${}^aX_N = \frac{R_N}{R_N + 1} \text{ and } {}^bX_N = \frac{1}{R_N + 1} \tag{3.8}$$

and in the spike:

$${}^aX_S = \frac{R_S}{R_S + 1} \text{ and } {}^bX_S = \frac{1}{R_S + 1} \tag{3.9}$$

Substituting Equations 3.9 and 3.8 into 3.7 yields:

$$N = S\frac{(R_N + 1)(R_S - R_m)}{(R_S + 1)(R_m - R_N)} \tag{3.10}$$

Equations 3.7 and 3.10 give the atomic concentration of X (in atoms/g). Dividing N by Avogadro's number N_A and multiplying with the atomic weights (g/mol) yields the corresponding weight percentages. Isotope dilution is a very powerful method because:

1. It does not require quantative separation of the elements of interest.

2. Chemical purification removes unwanted interferences from other species.

3. The method is very sensitive, so extremely low concentrations can be measured (ppb or less).

3.3 Sample-standard bracketing

Isotope dilution is the 'gold standard' for isotope geochemistry, recommended when the most accurate and precise results are desired. Unfortunately, isotope dilution is also very time consuming and cannot be readily applied to micro-analytical techniques such as LA-ICP-MS and SIMS. In those cases, and alternative method is used, which is less precise (%- rather than ‰- level precision) but quicker. The idea is to normalise the signal ratios recorded by the mass spectrometer to a standard of known age. As before, let P be a radioactive parent which decays to a radiogenic daughter D. Suppose that we can measure both nuclides on the same mass spectrometer, yielding two electronic signal intensities S_P and S_D. These signals may be recorded in units of V, A, or Hz. We cannot directly use the signal ratios as a proxy for the isotopic ratio:

$$\frac{N_D}{N_P} \neq \frac{S_D}{S_P}$$

because the parent and daughter are two different elements with different chemical properties and ionisation efficiencies. We can, however, assume that the isotopic ratio is proportional to the signal ratio:

$$\frac{N_D}{N_P} = C\frac{S_D}{S_P} \tag{3.11}$$

Thus, if we double N_D (and thus N_D/N_P), we would also expect to double S_D (and thus S_D/S_P). To determine the constant of proportionality C, we analyse a standard of known age (t_s) and, hence (N_D/N_P)-ratio (due to Equation 2.5):

$$C = \left(e^{\lambda_P t_s} - 1\right)\frac{S_P^s}{S_D^s} \tag{3.12}$$

where λ_P is the decay constant of the parent and S_P^s/S_D^s is the (inverse) signal ratio of the standard.

Chapter 4

Simple parent-daughter pairs

4.1 ^{14}C dating

There are two stable isotopes of carbon: ^{12}C and ^{13}C, and one naturally occurring radionuclide: ^{14}C. The half life of ^{14}C is only 5,730 years, which is orders of magnitude shorter than the age of the Earth. Therefore, no primordial radiocarbon remains and all ^{14}C is *cosmogenic* (see Section 8 for related methods). The main production mechanism is through secondary cosmic ray neutron reactions with ^{14}N in the stratosphere: $^{14}_{7}$N (n,p) $^{14}_{6}$C. Any newly formed ^{14}C rapidly mixes with the rest of the atmosphere creating a spatially uniform carbon composition, which is incorporated into plants and the animals that eat them. Prior to the industrial revolution, a gram of fresh organic carbon underwent 13.56 (β^-) decays per minute. When a plant dies, it ceases to exchange carbon with the atmosphere and the ^{14}C concentration decays with time according to Equation 2.2:

$$\frac{d^{14}C}{dt} = -\lambda_{14} \times {}^{14}C \tag{4.1}$$

where $\lambda_{14} = 0.120968$ ka^{-1}. Thus, the radiocarbon concentration is directly proportional to the radioactivity, which can be measured by β-counting. This can then be used to calculate the radiocarbon age by rearranging Equation 2.3:

$$t = -\frac{1}{\lambda_{14}} \ln \left[\frac{d^{14}C/dt}{(d^{14}C/dt)_\circ} \right] \tag{4.2}$$

where $(d^{14}C/dt)_\circ$ is the original level of β activity. This method was developed by Willard Libby in 1949, for which he was awarded the Nobel Prize in 1960. As mentioned before, $(d^{14}C/dt)_\circ$ was 13.56 prior to the industrial revolution, when thousands of tonnes of 'old' carbon were injected into the atmosphere, resulting in a gradual lowering of the radiocarbon concentration until 1950, when nuclear testing produced an opposite effect, leading to a doubling of the atmospheric ^{14}C activity in 1963. Since the banning of atmospheric nuclear testing, radiocarbon concentrations have steadily dropped until today, where they have almost fallen back to their pre-industrial levels. But even prior to these anthropogenic effects, ^{14}C concentrations underwent relatively large fluctuations as a result of secular variations of the Earth's magnetic field and, to a lesser extent, Solar activity. These variations in $(d^{14}C/dt)_\circ$ can be corrected by comparison with a precisely calibrated production rate curve, which was constructed by measuring the ^{14}C activity of tree rings (*dendrochronology*).

Since the 1980's, β-counting has been largely replaced by accelerator mass spectrometry (AMS, see Section 3.1), in which the ^{14}C concentration is measured directly relative to a stable isotope such as ^{13}C. Although this has not significantly pushed back the age range of the radiocarbon method, it has nevertheless revolutionised the technique by reducing the sample size requirements by orders of magnitude. It is now possible to analyse individual seeds or tiny fragments of precious objects such as the Turin Shroud, which was dated at AD1260-1390.

4.2 The Rb-Sr method

Trace amounts of Rb and Sr are found in most minerals as substitutions for major elements with similar chemical properties. Rb is an alkali metal that forms single valent positive ions with an ionic radius of 1.48 Å, which is similar to K^+ (1.33 Å). Rb is therefore frequently found in K-bearing minerals such as micas, K-feldspar and certain clay minerals. Strongly evolved alkalic rocks such as syenites, trachites and rhyolites often contain high Rb concentrations. Rb contains two isotopes of constant abundance: ^{85}Rb (72.1854%) and ^{87}Rb (27.8346%).

Sr is an alkaline earth metal that forms bivalent positive ions with a radius of 1.13 Å, similar to Ca^{2+} (ionic radius 0.99 Å). It therefore substitutes Ca^{2+} in many minerals such as plagioclase, apatite, gypsum and calcite in sites with 8 neighbours, but not in pyroxene where Ca^{2+} has a coordination number of 6. Native Sr^{2+} can also subsitute K^+ in feldspars (where radiogenic Sr is expected to be found), but this substitution is limited and requires the simultaneous replacement of Si^{4+} by Al^{3+} in order to preserve electric neutrality. Sr therefore predominantly occurs in Ca-rich undifferentiated rocks such as basalts. Sr contains four isotopes (^{84}Sr, ^{86}Sr, ^{87}Sr and ^{88}Sr) with variable abundance due to the variable amount of radiogenic ^{87}Sr. However, the non-radiogenic $^{84}Sr/^{86}Sr$ and $^{86}Sr/^{88}Sr$-ratios are constant with values of 0.056584 and 0.1194, respectively. The Rb-Sr chronometer is based on the radioactive decay of ^{87}Rb to ^{87}Sr:

$$^{87}Rb \rightarrow {}^{87}Sr + \beta^- + \nu + 0.275MeV \tag{4.3}$$

Where ν indicates an antineutrino. The number of radiogenic ^{87}Sr atoms produced by this reaction after a time t is given by:

$$^{87}Sr^* = {}^{87}Rb(e^{\lambda_{87}t} - 1) \tag{4.4}$$

where ^{87}Rb is the actual number of ^{87}Rb atoms per unit weight and λ_{87} is the decay constant 1.42 $\times$ 10^{-11} a^{-1} ($t_{1/2}$ = 4.88$\times 10^{10}$a). In addition to this radiogenic ^{87}Sr, most samples will also contain some 'ordinary' Sr. The total number of ^{87}Sr atoms measured is therefore given by:

$$^{87}Sr = {}^{87}Sr^* + {}^{87}Sr_\circ \tag{4.5}$$

with $^{87}Sr_\circ$ the initial ^{87}Sr present at the time of isotopic closure. Combining Equations 4.5 and 4.3, we obtain:

$$^{87}Sr = {}^{87}Sr_\circ + {}^{87}Rb(e^{\lambda_{87}t} - 1) \tag{4.6}$$

Dividing this by the non-radiogenic ^{86}Sr yields

$$\frac{^{87}Sr}{^{86}Sr} = \left(\frac{^{87}Sr}{^{86}Sr}\right)_\circ + \frac{^{87}Rb}{^{86}Sr}(e^{\lambda_{87}t} - 1) \tag{4.7}$$

The method can be applied to single minerals or to whole rocks. Given the very long half life, the optimal time scale ranges from the formation of the solar system to the late Palaeozoic (300-400 Ma). To

measure a Rb/Sr age, the weight percentage of Rb is measured by means of X-ray fluorescence, ICP-OES or similar techniques, and the $^{87}Sr/^{86}Sr$ ratio is determined by mass spectrometry (isotope dilution). The $^{87}Rb/^{86}Sr$-ratio is then calculated as:

$$\frac{^{87}Rb}{^{86}Sr} = \frac{Rb}{Sr}\frac{Ab(^{87}Rb)A(Sr)}{Ab(^{86}Sr)A(Rb)} \tag{4.8}$$

Where $Ab(\cdot)$ signifies 'abundance' and $A(\cdot)$ 'atomic weight'.

4.3 Isochrons

Equation 4.8 can be used in one of two ways. A first method is to use an assumed value for $(^{87}Sr/^{86}Sr)_\circ$, based on the geological context of the sample. This method is only reliable for samples with a high Rb/Sr ratio (e.g., biotite) because in that case, a wrong value for $(^{87}Sr/^{86}Sr)_\circ$ has only a minor effect on the age. A second and much better method is to analyse several minerals of the same sample and plot them on a $(^{87}Rb/^{86}Sr)$ vs. $(^{87}Sr/^{86}Sr)$ diagram (Figure 4.1). Due to Equation 4.7, this should form a linear array (the so-called *isochron*) with slope $(e^{\lambda_{87}t} - 1)$ and intercept $(^{87}Sr/^{86}Sr)_\circ$. Both parameters can be determined by linear regression, allowing us to quantify the 'goodness of fit' of the data and obviating the need to assume any initial Sr-ratios.

4.4 The Sm-Nd method

The elements Neodymium (Z=60) and Samarium (Z=62) are so-called 'rare earth elements'. All elements of this family have similar chemical properties. They nearly all form 3+ ions of roughly equal albeit slightly decreasing size with atomic number. The ionic radius of Nd and Sm is 1.08 and 1.04 Å, respectively. As the name suggests, rare earth elements rarely form the major constituents of minerals. One notable exception is monazite, which is a rare earth phosphate. In most cases, the rare earth elements are found in trace amounts of up to 0.1% in apatite [$Ca_5(PO_4)_3$(OH,Cl,F)] and zircon [$ZrSiO_4$]. Both Sm and Nd are slightly enriched in feldspar, biotite and apatite and thus tend to be found in higher concentrations in differentiated (alkalic) magmatic rocks.

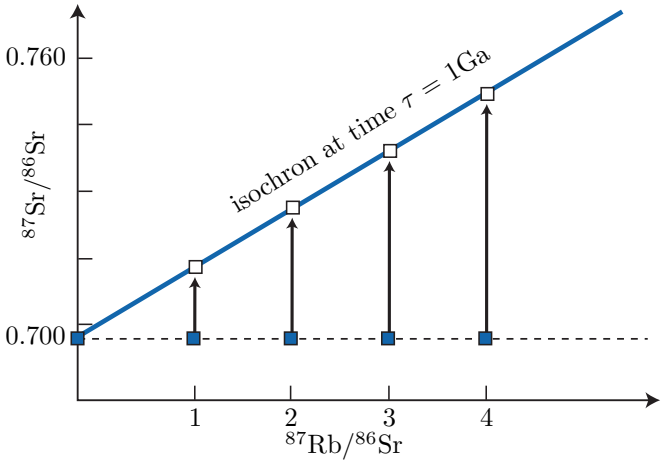

Figure 4.1: Schematic evolution of the $^{87}Sr/^{86}Sr$-system as a function of time for multiple aliquots of a hypthetical sample with initial ratio $(^{87}Sr/^{86}Sr)_\circ$=0.700. The slope of the isochron is a function of the age as per Equation 4.7 (modified from Allègre, 2008).

Because their chemical properties are so similar, geological processes are rarely capable of fractionating the Sm and Nd concentrations. Therefore, the Sm/Nd ratio in most rocks generally falls in a narrow range of 0.1 to 0.5 (the Sm/Nd ratio of the solar system being 0.31). One exception is garnet, in which Sm/Nd ratios > 1 have been found. Partial melting of mafic minerals such as pyroxene and olivine produces lower Sm/Nd ratios in the fluid phase than the solid residue. The Sm/Nd ratio of magmatic rocks therefore decreases with increasing differentiation.

Natural Sm contains seven naturally occurring isotopes, three of which are radioactive (^{147}Sm, ^{148}Sm and ^{149}Sm). Only ^{147}Sm has a sufficiently short half life to be useful for geochronology. Nd also contains seven isotopes, of which only one is radioactive (^{144}Nd) but with a very long half life. ^{143}Nd is the radiogenic daughter of ^{147}Sm and is formed by α-decay. This forms the basis of the Sm-Nd chronometer. Analogous to the Rb-Sr method (Equation 4.4), we can write:

$$^{143}Nd^{*} = {}^{147}Sm(e^{\lambda_{147}t} - 1) \tag{4.9}$$

Hence:

$$t = \frac{1}{\lambda_{147}} \ln\left(\frac{^{143}Nd^{*}}{^{147}Sm} + 1\right) \tag{4.10}$$

With $\lambda_{147} = 6.54{\times}10^{-12}a^{-1}$ ($t_{1/2} = 1.06{\times}10^{11}$a). Since most samples contain some initial Nd, the preferred way to calculate Sm/Nd ages is by analysing several minerals in a rock and create an isochron, similar to the Rb/Sr method (Section 4.3):

$$\frac{^{143}Nd}{^{144}Nd} = \left(\frac{^{143}Nd}{^{144}Nd}\right)_{\circ} + \frac{^{147}Sm}{^{144}Nd}\left(e^{\lambda_{147}t} - 1\right) \tag{4.11}$$

All measurements are done by mass spectrometry using isotope dilution. Because of the identical atomic masses of ^{147}Sm and ^{147}Nd, it is necessary to perform a chemical separation between Sm and Nd prior to analysis.

The Sm/Nd method is generally applied to basic and ultrabasic igneous rocks (basalt, peridotite, komatiite) of Precambrian to Palaeozoic age. The method thus complements the Rb/Sr method, which is preferentially applied to acidic rock types. The Sm/Nd method can also be applied to high grade metamorphic rocks (granulites, eclogites) as well as meteorites (shergottites, nahklites). Since the rare earths are significantly less mobile than Rb and Sr, the Sm/Nd is more reliable in rocks that have been disturbed by weathering or metamorphism.

Chapter 5

The U-Pb system

U and Th are found on the extremely heavy end of the Periodic Table of Elements. All their isotopes are radioactive and exhibit α-decay and sometimes even spontaneous fission (see Section 7.2). ^{232}Th, ^{235}U and ^{238}U each form the start of long decay series comprising multiple α- and β emissions which eventually produce various isotopes of Pb:

$$\begin{aligned} ^{238}U &\rightarrow \quad ^{206}Pb + 8\alpha + 6\beta + 47\text{MeV} \\ ^{235}U &\rightarrow \quad ^{207}Pb + 7\alpha + 4\beta + 45\text{MeV} \\ ^{232}Th &\rightarrow \quad ^{208}Pb + 6\alpha + 4\beta + 40\text{MeV} \end{aligned} \tag{5.1}$$

Each of these three decay series is unique, i.e. no isotope occurs in more than one series (Figure 2.2). Furthermore, the half life of the parent isotope is much longer than any of the intermediary daughter isotopes, thus fulfilling the requirements for secular equilibrium (Section 2.4). We can therefore assume that the ^{206}Pb is directly formed by the ^{238}U, the ^{207}Pb from the ^{235}U and the ^{208}Pb from the ^{232}Th. Several chronometers are based on the α-decay of U and Th:

- The U-Th-Pb method (Section 5.1)
- The Pb-Pb method (Section 5.2)
- The U-Th-He method (Section 7.1)

5.1 The U-(Th-)Pb method

Natural Pb consists of four isotopes ^{204}Pb, ^{206}Pb, ^{207}Pb and ^{208}Pb. The ingrowth equations for the three radiogenic Pb isotopes are given by:

$$\begin{aligned} {}^{206}Pb^* &= {}^{238}U\left(e^{\lambda_{238}t}-1\right) \\ {}^{207}Pb^* &= {}^{235}U\left(e^{\lambda_{235}t}-1\right) \\ {}^{208}Pb^* &= {}^{232}Th\left(e^{\lambda_{232}t}-1\right) \end{aligned} \tag{5.2}$$

With $\lambda_{238} = 1.551359 \times 10^{-10} a^{-1}$ ($t_{1/2} = 4.468$ Gyr), $\lambda_{235} = 9.845841 \times 10^{-10} a^{-1}$ ($t_{1/2} = 703.8$ Myr), and $\lambda_{232} = 0.4933431 \times 10^{-10} a^{-1}$ ($t_{1/2} = 14.05$ Gyr). The corresponding age equations are:

$$\begin{aligned} t_{206} &= \frac{1}{\lambda_{238}} \ln\left(\frac{^{206}Pb^*}{^{238}U}+1\right) \\ t_{207} &= \frac{1}{\lambda_{235}} \ln\left(\frac{^{207}Pb^*}{^{235}U}+1\right) \\ t_{208} &= \frac{1}{\lambda_{232}} \ln\left(\frac{^{208}Pb^*}{^{232}Th}+1\right) \end{aligned} \tag{5.3}$$

Some igneous minerals (notably zircon) conveniently incorporate lots of U and virtually no Pb upon crystallisation. For those minerals, the non-radiogenic Pb can be safely neglected (at least for relatively young ages), so that we can assume that $Pb \approx Pb^*$. This assumption cannot be made for other minerals, young ages, and high precision geochronology. In those cases, the inherited component (aka 'common Pb') needs to be quantified, which is done by normalising to non-radiogenic ^{204}Pb:

$$\begin{aligned} \frac{^{206}Pb}{^{204}Pb} &= \left(\frac{^{206}Pb}{^{204}Pb}\right)_\circ + \frac{^{238}U}{^{204}Pb}\left(e^{\lambda_{238}t}-1\right) \\ \frac{^{207}Pb}{^{204}Pb} &= \left(\frac{^{207}Pb}{^{204}Pb}\right)_\circ + \frac{^{235}U}{^{204}Pb}\left(e^{\lambda_{235}t}-1\right) \\ \frac{^{208}Pb}{^{204}Pb} &= \left(\frac{^{208}Pb}{^{204}Pb}\right)_\circ + \frac{^{232}Th}{^{204}Pb}\left(e^{\lambda_{232}t}-1\right) \end{aligned} \tag{5.4}$$

where $\left(\frac{^{x}Pb}{^{204}Pb}\right)_\circ$ stands for the common Pb component for isotope x. The corresponding age equations then become:

$$\left.\begin{aligned} t_{206} &= \frac{1}{\lambda_{238}} \ln\left(\frac{\left(\frac{^{206}Pb}{^{204}Pb}\right)-\left(\frac{^{206}Pb}{^{204}Pb}\right)_\circ}{\frac{^{238}U}{^{204}Pb}}+1\right) \\ t_{207} &= \frac{1}{\lambda_{235}} \ln\left(\frac{\left(\frac{^{207}Pb}{^{204}Pb}\right)-\left(\frac{^{207}Pb}{^{204}Pb}\right)_\circ}{\frac{^{235}U}{^{204}Pb}}+1\right) \\ t_{208} &= \frac{1}{\lambda_{232}} \ln\left(\frac{\left(\frac{^{208}Pb}{^{204}Pb}\right)-\left(\frac{^{208}Pb}{^{204}Pb}\right)_\circ}{\frac{^{232}Th}{^{204}Pb}}+1\right) \end{aligned}\right. \tag{5.5}$$

U-Pb dating grants access to two separate geochronometers (^{206}Pb/^{238}U and ^{207}Pb/^{235}U) based on different isotopes of the same parent-daughter pair (i.e. U & Pb). This built-in redundancy provides a powerful internal quality check which makes the method arguably the most robust and reliable dating technique in the geological toolbox. The initial Pb composition can either be determined by analysing the Pb composition of a U-poor mineral (e.g., galena or feldspar) or by applying the isochron method to samples with different U and Th concentrations. As is the case for any isotopic system, the system needs to remain 'closed' in order to yield meaningful isotopic ages. This sometimes is not the case, resulting in a loss of Pb and/or U. Such losses cause the ^{206}Pb/^{238}U- and ^{207}Pb/^{235}U-clocks to yield different ages. Note that isotopic closure is required for all intermediary isotopes as well. Critical isotopes are the highly volatile ^{226}Rn ($t_{1/2}$=1.6ka) and ^{222}Rn ($t_{1/2}$=3.8d). Initially, the U-Pb method was applied to U-ores, but nowadays it is predominantly applied to accessory minerals such zircon and, to a lesser extent, apatite, monazite and allanite.

5.2 The Pb-Pb method

The ^{207}Pb/^{206}Pb method is based on the U-Pb method and is obtained by dividing the two U-Pb members of Equation 5.2 (or 5.4), and taking into account that the natural ^{238}U/^{235}U-ratio is 137.88:

$$\frac{^{207}Pb^*}{^{206}Pb^*} = \frac{\left(\frac{^{207}Pb}{^{204}Pb}\right)-\left(\frac{^{207}Pb}{^{204}Pb}\right)_\circ}{\left(\frac{^{206}Pb}{^{204}Pb}\right)-\left(\frac{^{206}Pb}{^{204}Pb}\right)_\circ} = \frac{1}{137.88}\frac{e^{\lambda_{235}t}-1}{e^{\lambda_{238}t}-1} \tag{5.6}$$

The left hand side of this equation contains only Pb isotopic ratios. Note that these are *only* a function of time. Equations 5.6 has no direct solution and must be solved iteratively. The Pb-Pb method has the following advantages over conventional U-Pb dating:

- There is no need to measure uranium.
- The method is insensitive to recent loss of U and even Pb, because this would not affect the isotopic ratio of the Pb.

In practice, the Pb-Pb method is rarely applied by itself but is generally combined with the U-Pb technique. The expected $(^{207}Pb/^{206}Pb)^*$-ratio for recently formed rocks and minerals can be calculated from Equation 5.6 by setting t→0:

$$\left(\frac{^{207}Pb}{^{206}Pb}\right)^*_p = \frac{\lambda_{235}}{137.88\lambda_{238}} = 0.04604 \tag{5.7}$$

This ratio was progressively higher as one goes back further in time. It was ≈ 0.6 during the formation of Earth.

5.3 Concordia

It sometimes happens that the U-Th-Pb trio of chronometers does not yield mutually consistent ages. It is then generally found that $t_{208} < t_{206} < t_{207} < t_{207/206}$ which, again, shows that the Pb-Pb clock is least sensitive to open system behaviour. From Equation 5.2, we find that:

$$\begin{array}{ll} \frac{^{206}Pb^*}{^{238}U} & = e^{\lambda_{238}t} - 1 \text{ and} \\ \frac{^{207}Pb^*}{^{235}U} & = e^{\lambda_{235}t} - 1 \end{array} \tag{5.8}$$

If we plot those $^{206}Pb^*/^{238}U$- and $^{207}Pb^*/^{235}U$-ratios which yield the same ages (t) against one another, they form a so-called 'concordia' curve. The concordia diagram is a very useful tool for investigating and interpreting disruptions of the U-Pb system caused by 'episodic lead loss'. This means that a mineral (of age $T_\circ$, say) has lost a certain percentage of its radiogenic Pb at a time T_1 after its formation (e.g., during metamorphism), after which the system closes again and further accumulation of radiogenic Pb proceeds normally until the present. On the concordia diagram of multiple aliquots of a sample, this scenario will manifest itself as a linear array of datapoints connecting the concordant $^{206}Pb^*/^{238}U$ - $^{207}Pb^*/^{235}U$ composition expected at $T_\circ$ with that expected at T_1. With time, the data shift further away from the origin. The upper intercept of the linear array (aka *discordia* line) can be used to estimate the crystallisation age, whereas the lower intercept yields the age of metamorphism. The greater the distance from the

expected composition at t, the greater the degree of Pb loss and the greater the linear extrapolation error on the crystallisation age (Figure 5.1).

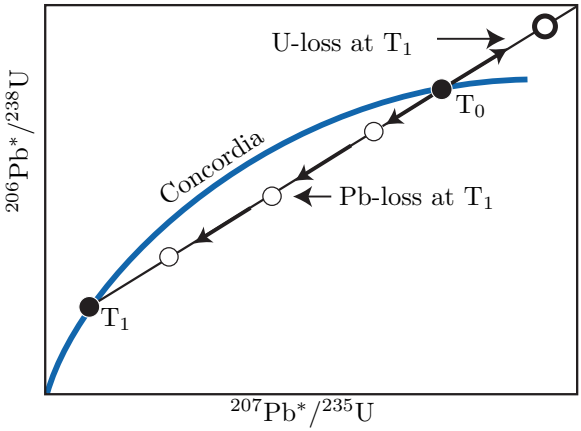

Figure 5.1: 'Wetherill' concordia diagram showing concordant (filled symbols) and discordant (empty symbols) analyses affected by different degrees of Pb (or U) loss (modified from Allègre, 2008).

5.4 Detrital geochronology

Zircon ($ZrSiO_4$) is a common U-Th-bearing accessory mineral in acidic igneous rocks, which form the main proto-sources of the siliciclastic sediments. Zircon is a very durable mineral that undergoes minimal chemical alteration or mechanical abrasion. Therefore, zircon crystals can be considered time capsules carrying the igneous and metamorphic history of their proto-sources. The probability distribution of a representative sample of zircon U-Pb ages from a detrital population can serve as a characteristic fingerprint that may be used to trace the flow of sand through sediment routing systems. As a provenance tracer, zircon U-Pb data are less susceptible to winnowing effects than conventional petrographic techniques. Using modern microprobe technology (SIMS and LA-ICP-MS, see Chapter 3.1), it is quite easy to date, say, a hundred grains of zircon in a matter of just a few hours. Due to the

robustness of zircons as a tracer of sedimentary provenance, and the relative ease of dating them, the use of detrital zircon U-Pb geochronology has truly exploded in recent years. A literature survey using the keywords 'detrital', 'zircon', and 'provenance' indicates that the proliferation of detrital zircon studies has followed an exponential trend, with the number of publications doubling roughly every five years over the past two decades. At present, nearly a thousand detrital zircon publications appear each year.

An extensive survey of late Archaean sandstones from the Jack Hills in Australia have revealed a subpopulation of detrital zircons with Hadean (4.1-4.2 Ga) U-Pb ages. These are the oldest terrestrial minerals known to science, predating the oldest igneous rocks by 300 million years. The isotopic composition of oxygen, hafnium and other elements in the zircon represents a unique window into the earliest stages of Earth evolution. They indicate that liquid water was present on the surface of our planet early on in its history. This isotopic evidence is corroborated by the geological observation that the Hadean zircons are preserved in fluvial deposits.

Chapter 6

The K-Ar system

Potassium has three naturally occurring isotopes: ^{39}K, ^{40}K and ^{41}K. ^{40}K is radioactive and undergoes branched decay to ^{40}Ca (by electron emission $\lambda_{\beta-} = 4.962 \times 10^{-10} yr^{-1}$) and ^{40}Ar (by electron capture $\lambda_e = 0.581 \times 10^{-10} yr^{-1}$) with a combined half life of 1.248 billion years. The positron emission mechanism mentioned in Chapter 2.2 has an extremely long half life and can therefore safely be neglected. In addition to ^{40}Ar, argon has two more stable isotopes: ^{36}Ar and ^{38}Ar. Argon makes up ∼1% of the terrestrial atmosphere, with a fixed isotopic composition of ^{40}Ar/^{36}Ar = 295.5 and ^{38}Ar/^{36}Ar = 0.187. The argon contained in K-bearing minerals is made up of a mixture of radiogenic (^{40}Ar*) and non-radiogenic gas (^{40}Ar$_\circ$):

$$\begin{aligned} {}^{40}Ar &= {}^{40}Ar_\circ + {}^{40}Ar^* \\ \text{where } {}^{40}Ar^* &= \tfrac{\lambda_e}{\lambda} {}^{40}K \left(e^{\lambda t} - 1\right) \end{aligned} \tag{6.1}$$

with λ the total decay constant of ^{40}K ($\lambda = \lambda_e + \lambda_{\beta-} = 5.543 \times 10^{-10} yr^{-1}$).

6.1 K-Ar dating

The $^{40}\text{K} \rightarrow {}^{40}\text{Ar}^*$ decay scheme forms the basis of the K-Ar geochronometer, with the following age equation:

$$t = \frac{1}{\lambda} \ln \left[1 + \frac{\lambda}{\lambda_e} \left(\frac{{}^{40}Ar^*}{{}^{40}K} \right) \right] \tag{6.2}$$

Taking into account the 'contaminated' (aka 'excess' or 'inherited') argon component $^{40}Ar_\circ$ and analysing several cogenetic rocks or minerals with different K (and therefore $^{40}Ar^*$) contents, an *isochron* equation can be formed by division through ^{36}Ar:

$$\frac{^{40}Ar}{^{36}Ar} = \left(\frac{^{40}Ar}{^{36}Ar}\right)_\circ + \frac{\lambda_e}{\lambda}\frac{^{40}K}{^{36}Ar}\left(e^{\lambda t} - 1\right) \tag{6.3}$$

which can be solved for t. Alternatively, we can simply assume that all the inherited argon has an atmospheric origin, so that $(^{40}Ar/^{36}Ar)_\circ = 295.5$.

6.2 ^{40}Ar/^{39}Ar dating

From an analytical perspective, K-Ar dating is a two step process. Because K (an alkali metal) and Ar (a noble gas) cannot be measured on the same analytical equipment, they must be analysed separately on two different aliquots of the same sample. This limitation is overcome by the ^{40}Ar/^{39}Ar technique, which is a clever variation of the K-Ar method. The idea is to subject the sample to neutron irradiation and convert a small fraction of the ^{39}K to synthetic ^{39}Ar, which has a half life of 269 years. The age equation can then be rewritten as follows:

$$t_x = \frac{1}{\lambda}\ln\left[1 + J\left(\frac{^{40}Ar^*}{^{39}Ar}\right)_x\right] \tag{6.4}$$

where 'x' stands for 'sample' and J is a constant of proportionality which encapsulates the efficiency of the ^{39}K (n,p) ^{39}Ar reaction and into which the factor λ/λ_e is folded as well. The J-value can be determined by analysing a standard of known age t_s which was co-irradiated with the sample:

$$t_s = \frac{1}{\lambda}\ln\left[1 + J\left(\frac{^{40}Ar^*}{^{39}Ar}\right)_s\right] \tag{6.5}$$

In which the subscript 's' stands for 'standard'. The great advantage of equation 6.4 over 6.2 is that all measurements can be completed on the same aliquot and using a single instrument, namely a noble gas mass spectrometer, which can analyse extremely small (down to μg-sized) samples.

The ^{40}Ar/^{39}Ar-method also allows the analyst to investigate the extent of *argon loss* by means of stepwise heating experiments. This is done by degassing the sample under ultra-high vacuum conditions in a resistance furnace. At low temperatures, the weakly bound Ar is released, whereas the strongly bound Ar is released from the crystal lattice at high temperatures until the sample eventually melts. Plotting the *apparent ages* against the cumulative fraction of ^{39}Ar released yields an ^{40}Ar/^{39}Ar age spectrum (Figure 6.1). If a rock or mineral has remained closed since its formation, the ^{40}Ar/^{39}Ar-ratio should remain constant over the course of the different heating steps, forming an 'age plateau'. More complex (e.g. rising) release spectra, on the other hand, are diagnostic of complex thermal histories featuring partial argon loss. 'saddle' shaped release spectra are indicative of 'excess' argon. The composition of the inherited argon gas can be determined using a variant of the isochron method, assuming that all ^{36}Ar is inherited:

$$\frac{^{40}Ar}{^{36}Ar} = \left(\frac{^{40}Ar}{^{36}Ar}\right)_{\circ} + \frac{^{39}Ar}{^{36}Ar}\frac{e^{\lambda t}-1}{J} \tag{6.6}$$

If the Ar contamination is constant throughout the entire sample, then the $\frac{^{40}Ar}{^{36}Ar}$-measurements will be arranged along a linear trend whose slope is a function of $\frac{^{40}Ar^*}{^{39}Ar}$ and, hence, the age.

6.3 Applications

The K-Ar and ^{40}Ar/^{39}Ar-methods are some of the most widely used geochronometers and important tools in the calibration of the geologic time scale. The method is applicable to rocks and minerals $> 10^6$yr. Obviously, younger materials require more careful treatment of the inherited argon components.

- Magmatic rocks: formation ages can only be obtained for rapidly cooled volcanic rocks, using either mineral separates (sanidine, biotite, hornblende) or whole rocks. Pyroclastics and obsidian may yield reliable ages only if they are unaltered and contain little non-radiogenic argon. Plutonic rocks typically cool much slower than volcanic rocks and generally yield cooling ages rather than formation ages.

- Sedimentary rocks: K-Ar dating of *authigenic* mineral phases has often been attempted but remains difficult. Glauconite has been

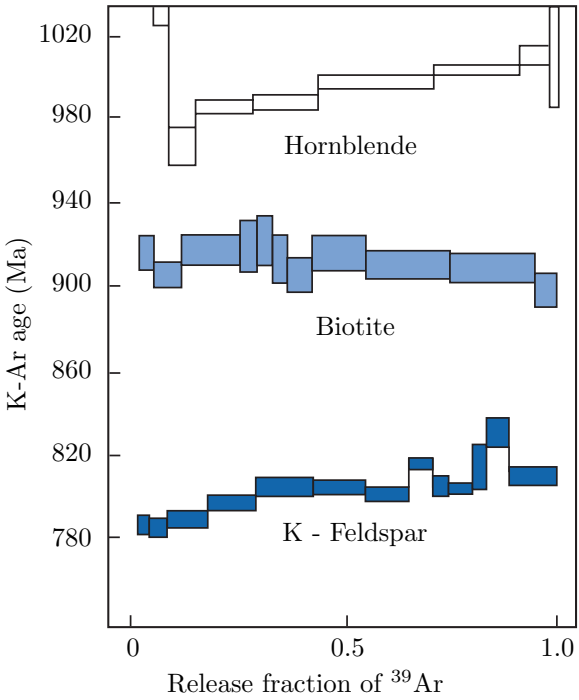

Figure 6.1: $^{40}Ar/^{39}Ar$ age spectra obtained by stepwise heating of three different K-bearing minerals. Biotite exhibits a flat 'plateau', indicating a simple history of rapid crystallisation and/or cooling. K-feldspar shows a rising age spectrum, consistent with a more complex evolution comprising multiple growth phases and/or thermal resetting. Finally, hornblende shows a 'U-shaped' release spectrum in which the first heating step releases a large amount of 'excess' argon (modified from Allègre, 2008).

used successfully in some cases. Dating detrital minerals such as white mica (muscovite, phengite) in fluvial sediments is frequently used to study the metamorphic history of the hinterland.

- Metamorphic rocks: pelitic metamorphic rocks tend to be rich in K-bearing micas and amphiboles, which can easily be dated with the K-Ar and $^{40}Ar/^{39}Ar$ methods, but require careful interpretation. In high grade metamorphic terranes, the apparent

ages can either reflect the metamorphic crystallisation history or the postmetamorphic cooling history. Low grade metamorphic terranes, on the other hand, carry a risk of containing inherited argon components from previous evolutionary stages.

Chapter 7

Thermochronology

The temperature sensitivity of the K-Ar system (Section 6) is a characteristic feature not only of this method, but of a separate class of geochronometers known as 'thermochronometers'. The most important of these methods are the U-Th-He 7.1 and fission track 7.2 techniques, which are becoming increasingly popular as a means of investigating Earth surface processes.

7.1 The U-Th-He method

When U and Th decay to various isotopes of Pb (Section 5.1), they do so by α-emission (Section 2.2). When α particles acquire electrons, they become helium atoms. Thus, not only Pb content, but also the He content increases relative to U and Th through time, forming the basis of the U-Th-He chronometer:

$$\begin{aligned} {}^4He = \quad & \left[8\tfrac{137.88}{138.88}(e^{\lambda_{238}t}-1) + 7\tfrac{1}{138.88}(e^{\lambda_{235}t}-1)\right]U + \\ & 6(e^{\lambda_{232}t}-1)Th + 0.1499(e^{\lambda_{147}t}-1)Sm \end{aligned} \tag{7.1}$$

Where the values '8', '7' and '6' refer to the number of α-particles produced in the decay chains of ^{238}U, ^{235}U and ^{232}Th, respectively (Figure 2.2), 137.88 is the (constant) ratio of naturally occurring ^{238}U and ^{235}U, and the last term accounts for the (often negligible) accumulation of helium by Sm-decay (Section 4.4). It was Ernest Rutherford who first proposed that the U-Th-He decay scheme could be used as an

absolute dating technique, making it the oldest radiometric chronometer. Early experiments on uraninite (UO_2) by Robert John Strutt (4^{th} Baron Rayleigh) at Imperial College London in 1905 yielded ages that were systematically too young. This was correctly attributed to the volatile nature of the helium atom, which diffuses out of most minerals at low temperatures and therefore yields only *minimum ages*. As a result, the method was largely abandoned until 1987, when American geochronologist Peter Zeitler realised that this 'leaky' behaviour provided a powerful means of reconstructing the thermal evolution of rocks and minerals.

Let C(x,y,z) be the He-concentration as a function of the spatial coordinates x, y and z. The evolution of C with time (t) is given by the diffusion equation ('Fick's law'):

$$\frac{\partial C}{\partial t} = D\left(\frac{\partial^2 C}{\partial x^2} + \frac{\partial^2 C}{\partial y^2} + \frac{\partial^2 C}{\partial z^2}\right) \tag{7.2}$$

Where D is the 'diffusion coefficient', which varies exponentially with temperature (T) according to the 'Arrhenius Law':

$$D = D_\circ e^{-\frac{E_a}{RT}} \tag{7.3}$$

with $D_\circ$ the 'frequency factor', E_a the 'activation energy' and R the ideal gas constant (8.3144621 J/mol.K). By taking the logarithm of both sides of Equation 7.3, we obtain (Figure 7.1):

$$\ln(D) = \ln(D_\circ) - \frac{E_a}{RT} \tag{7.4}$$

Both the frequency factor and the activation energy can be determined from *diffusion experiments*, in which a He-bearing mineral is subjected to a step-heating experiment similar to the kind we saw in the $^{40}Ar/^{39}Ar$ method (Section 6.2).

Let us now consider the situation of a mineral which (a) accumulates He through radioactive decay of U and Th, (b) loses He by thermal diffusion, and (c) undergoes monotonic cooling at a variable rate dT/dt. At high temperatures, the He will be lost quickly but as time progresses, the thermal diffusion becomes increasingly sluggish until the He is eventually 'locked' into the crystal lattice and the istopic system

is effectively *closed*. If the thermal history is so that 1/T increases linearly with time, then it is possible to calculate an equivalent 'closure temperature' T_c. This is known as 'Dodson's equation':

$$\frac{E_a}{RT_c} = \ln\left(\frac{ART_c^2 D_\circ / r^2}{E_a dT/dt}\right) \tag{7.5}$$

where r = is the effective grain size (radius) of the mineral and A is a geometric factor (55 for a sphere, 27 for a cylinder and 8.7 for a plane sheet). Thus the U-Th-He age calculated at the end of the aforementioned thermal history equals that which would have been obtained if He accumulated linearly since the rock passed through T_c.

Although the closure temperature concept is an oversimplication of reality, it has great intuitive appeal. Consider, for example, a vertical transect in a rapidly exhuming mountain range. The *apparent* U-Th-He ages along such a transect are approximately given by the time elapsed since the respective rocks have passed through T_c. For apatite [$Ca_5(PO_4)_3$(OH,F,Cl)], this is $\sim 60°C$, which corresponds to a depth (assuming a thermal gradient of 30°C/km) of 1.5-2km. Thus, the rocks at the high elevations along the transect will have passed through T_c before those collected at the bottom of the transect, and the corresponding U-Th-He ages will therefore increase with elevation. Moreover, the rate of increase of age increase with elevation can be used to estimate the *exhumation rate* of the orogen.

7.2 Fission tracks

In addition to α, β and γ decay, which form the basis of the U-Th-Pb (Section 5) and U-Th-He (Section 7.1) methods, a tiny fraction (1/1,000,000) of the ^{238}U atoms decay by *spontaneous fission* (Section 2.2). In this decay mechanism, the parent nuclide (i.e., ^{238}U) decays into two daughter nuclides of roughly equal mass (e.g., Ba and Kr). These two particles carry a large amount of energy ($\sim$ 170 MeV) and, having a positive charge, strongly repel each other. Each of the two fission fragments travels through the crystal lattice of the host mineral, leaving a trail of damage behind. Although fission tracks can be directly observed by transmission electron microscopy (TEM), a more practical approach is to etch (a polished surface of) the host mineral with acid. This enlarges the damage zones and makes it possible to count them

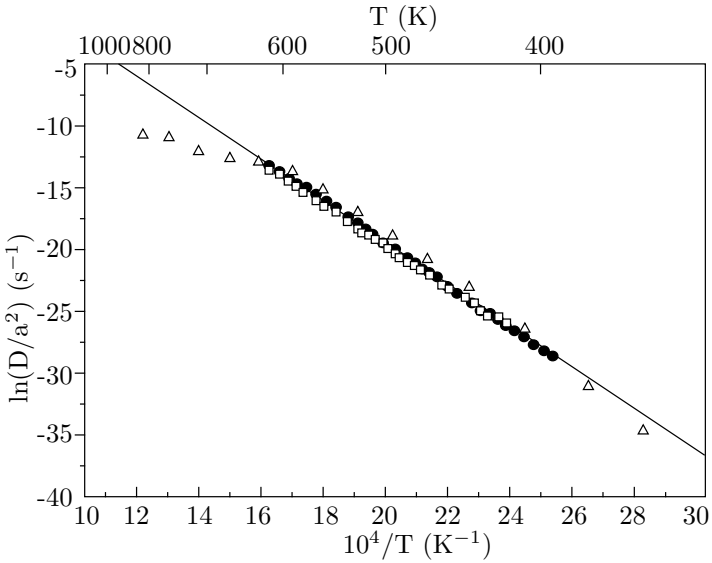

Figure 7.1: 'Arrhenius' diagram of three step-heating experiments of ^{4}He in apatite, showing simple diffusion behaviour in agreement with Equation 7.3. Extrapolating the linear trend to geological time scales yields a 'closure temperature' of ∼60°C (Equation 7.5). Modified from Braun et al. (2006).

under an ordinary petrographic microscope. The volume density N_s (in cm^{-3}) of the fission tracks is given by:

$$N_s = \frac{\lambda_f}{\lambda}[^{238}U]\left(e^{\lambda t} - 1\right) \tag{7.6}$$

where $[^{238}U]$ stands for the volume density the ^{238}U atoms, λ_f is the fission decay constant (8.46×10^{-17}yr^{-1}) and λ is the total decay constant of ^{238}U (1.55125×10^{-10}yr^{-1}, see Section 5). The (unobservable) volume density of the tracks is related to the (observable) surface density ρ_s (in cm^{-2}) by:

$$\rho_s = gLN_s \tag{7.7}$$

Where g is geometry factor (g=1 if determined on an internal and g=1/2 on an external surface) and L is the etchable length of a fission track (∼15μm). Rearranging Equation 7.6 for time:

$$t = \frac{1}{\lambda} \ln \left(\frac{\lambda}{\lambda_f} \frac{\rho_s}{[^{238}U] g L} + 1 \right) \tag{7.8}$$

In practice, $[^{238}U]$ is determined by irradiating the (etched) sample with thermal neutrons in a reactor. This irradiation induces synthetic fission of ^{235}U in the mineral (Equation 2.1). These tracks can be monitored by attaching a mica detector to the polished mineral surface and etching this monitor subsequent to irradiation (Figure 7.2). The surface density of the induced tracks in the mica detector (ρ_i) is a function of the nuclear cross section of the neutron-induced fission reaction on ^{235}U and the neutron fluence in the reactor, both of which are unknown. A pragmatic solution to this problem is found by irradiating the sample along with a standard of known age, and lumping all the unknown parameters together into a calibration factor (ζ), so that the age of the sample reduces to:

$$t = \frac{1}{\lambda} \ln \left(1 + \frac{g_i}{g_s} \lambda \zeta \rho_d \frac{\rho_s}{\rho_i} \right) \tag{7.9}$$

where $g_s = 1$, $g_i = 1/2$ and ρ_d is the surface density of the induced fission tracks in a dosimeter glass of known (and constant) U concentration. The latter value is needed to 'recycle' the ζ value from one irradiation batch to the next, as neutron fluences might vary through time, or within a sample stack.

Laboratory experiments have revealed that fission tracks are sensitive to heat. For example, it suffices that apatite is heated to 500°C for 1 hour for all the latent fission tracks to anneal. Moderate heating shortens the tracks and reduces their surface density and, hence, the apparent age of the sample. In boreholes, the apparent fission track age remains constant until a depth is reached where the ambient temperature is high enough for the tracks to be reduced in size and number. This region is called the *Partial Annealing Zone* (PAZ). Below the PAZ, no tracks are retained (Figure 7.3). The reduction of the surface density of the spontaneous tracks per unit time can be written as a function of temperature (T, in Kelvin):

$$\frac{d\rho_s}{dt} = -C \rho_s e^{-E_a/kT} \tag{7.10}$$

where C is a material constant, E_a is the activation energy for track shortening and k is the Boltzmann constant (8.616×10^{-5}eV/K).

Integration of Equation 7.10 yields:

$$\ln\left(\frac{\rho_\circ}{\rho}\right) = C\ t\ e^{-E_a/kT} \tag{7.11}$$

where $\rho_\circ$ is the initial track density prior to heating. Taking logarithms:

$$\ln(t) = \frac{E_A}{kT} + \ln\left[\ln\left(\frac{\rho_\circ}{\rho}\right)\right] - \ln(C) \tag{7.12}$$

For any given *retention coefficient* $\rho_\circ/\rho$, there exists a linear relationship between ln(t) and 1/T. This is an *Arrhenius trend* similar to the one described by Equation 7.3 in the context of U-Th-He thermochronology. By extrapolating the Arrhenius diagram to long time scales ($t \sim 10^6$yr), it is possible to calculate a 'closure temperature' T_c similar to that which is calculated for the U-Th-He system. For apatite, $\mathrm{T}_c \approx 100°C$, whereas for zircon, $\mathrm{T}_c \approx 240°C$.

If a sample has spent some of its time inside the PAZ, then the subpopulation of its fission tracks formed during that thime will be shorter than those that subsequently formed above the PAZ. The probability distribution of the fission track lengths can be determined by measuring the distance between the two tips of a large number of (100, say) *horizontally confined* fission tracks under the optical microscrope. Sophisticated inverse modelling algorithms have been developed to interpret these length distributions and extract continuous time-temperature (t-T) paths from them. Such modelling exercises have become an integral part of modern fission track studies.

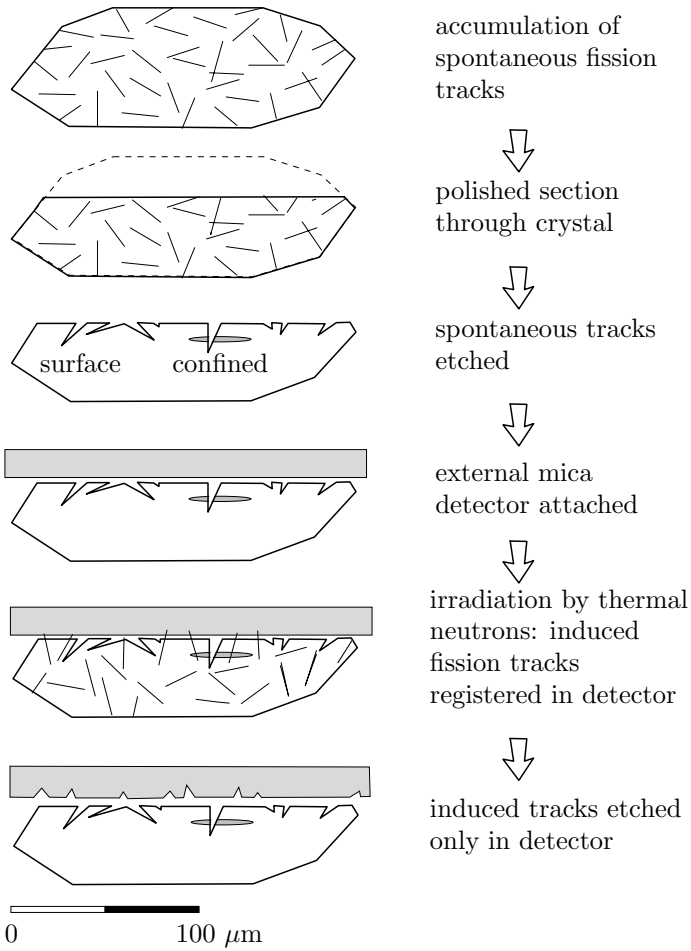

Figure 7.2: Schematic diagram illustrating the external detector method for fission track geochronology (modified from Galbraith, 2005).

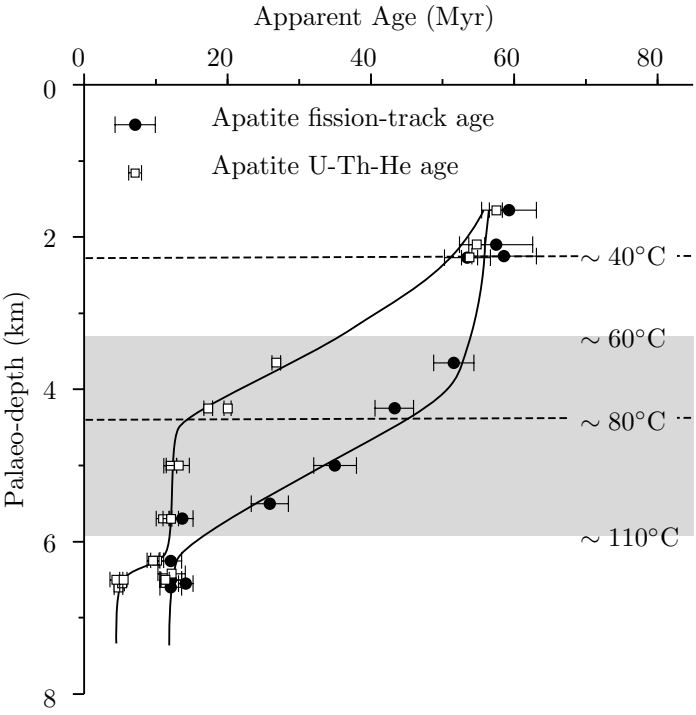

Figure 7.3: Vertical profile of U-Th-He and fission track ages in apatite, collected along the footwall of an exhumed normal fault block in the White Mountains of eastern California. Samples at the highest elevations have resided at shallow depths for up to 55 Myr. Dashed lines show the extent of the 'Partial Retention Zone' (PRZ), in which apatite has partially lost its radiogenic helium. The grey area indicates the 'Partial Annealing Zone', where fission tracks have been shortened. At low elevations, young ages are observed, indicating rapid exhumation by the normal fault at 12 Ma. Additionally, the U-Th-He data show a hint of a second exhumation phase at 5 Ma (modified from Stockli, Farley and Dumitru, 2000, *Geology* v. 28, no. 11, p. 983-986).

Chapter 8

Cosmogenic nuclide geochronology

The Earth is constantly bombarded by galactic cosmic rays, which primarily consist of protons. Many of these electrically charged particles never reach our planet because they are deflected back into space by the Earth's magnetic field (see Equation 3.3). The degree of 'protection' provided by the magnetic field is greater at low latitudes (where the magnetic field lines run parallel to the surface) than at the poles (where they are perpendicular to the surface). Thus, the cosmic ray intensity at the equator is significantly lower than at the poles, although the average energy (or 'rigidity') of the cosmic rays is higher[1]

The primary cosmic rays which do manage to pass through the magnetic field strongly interact with the atmosphere and form a secondary cosmic ray 'shower', which is mostly made of neutrons and muons. This secondary cosmic ray shower is rapidly attenuated as it travels down into the atmosphere. Only a very small fraction of the secondary cosmic rays, which mostly consist of neutrons, reach the surface of the Earth. These neutrons then collide with the elements that are found in rocks and soils, such as silicon, oxygen, calcium etc. When such an element is hit by a cosmic ray, it undergoes 'spallation', which basically means that it explodes into smaller particles. Most of these particles

[1] At the poles, even low energy solar cosmic rays (which predominantly consist of electrons, not protons) can reach the upper atmosphere, giving rise to the Aurora Borealis.

are either very short lived or very common in the Earth's crust. But some of the spallation products are very rare yet sufficiently long lived to accumulate in measurable quantities in terrestrial rocks. One example is ^{10}Be, which has a half life of 1.3 million years. This is orders of magnitude shorter than the age of the Earth. So, just like the ^{14}C discussed in Section 4.1, the existence of ^{10}Be on our planet would be impossible to explain without these cosmogenic production pathways.

The production of *cosmogenic nuclides* is restricted to the uppermost few meters below the surface. So if the concentration of the ^{10}Be in the surface rocks is known, and if the production rate is known, then the exposure age of the rock can be estimated. This is similar to measuring how long a person has been exposed to sunlight by measuring the tan of their skin. During the 20 years or so that cosmogenic nuclide geochronology has been around, it has truly revolutionised various aspects of geomorphology, such as the study of volcanoes, river incision, landslides, glaciers, sediments, and faults.

nuclide	half life	reaction types	target minerals
^{3}He	stable	spallation on O, Si	olivine, pyroxene
^{21}Ne	stable	spallation on Mg, Fe	quartz
^{10}Be	1.36 Myr	^{16}O(n,4p3n)^{10}Be	quartz
		^{28}Si(n,x)^{10}Be	
^{26}Al	717 kyr	^{28}Si(n,p2n)^{26}Al	quartz
^{36}Cl	301 kyr	^{40}Ca(n,2n3p)^{36}Cl	calcite, plagioclase
		^{39}K(μ^-,p2n)^{36}Cl	
		^{40}Ca(μ^-,α)^{36}Cl	
		^{35}Cl(n,μ)^{36}Cl	
^{14}C	5730 yr	^{16}O(n,2pn)^{14}C	quartz

Table 8.1: Commonly used terrestrial cosmogenic nuclides.

Table 8.1 lists the most commonly used cosmogenic nuclides. What all these isotopes have in common is that they are normally absent from rocks that are shielded from cosmic rays. They belong to two categories. There are the cosmogenic noble gases, which are stable, and the cosmogenic radionuclides, which are radioactive. Each of these have different applications.

8.1 Stable nuclides

In the simplest case of a stable nuclide in the absence of erosion, its concentration increases linearly with time (t). So if we measure the concentration (N) in atoms per gram of, say, quartz, and if we know the production rate (P), in atoms per gram per year, then we can simply calculate the age by dividing the concentration by the production rate:

$$t = \frac{N}{P} \tag{8.1}$$

Next, consider the situation of a stable nuclide and a rock surface that is in steady state erosion. To understand this situation, it is useful to imagine one in the place of a rock particle under an eroding surface. As the particle approaches the surface, it sees an exponentially increasing cosmic ray intensity and cosmogenic nuclide production rate. So in the case of an eroding surface, the cosmogenic nuclide content can be used not to measure an exposure age, but an erosion rate (ϵ). ϵ is a simple function of the production rate P and the concentration N, multplied by a factor Λ/ρ, where ρ is the rock density and Λ is the attenuation length ($\sim$160 g/cm^{-2}). This factor quantifies how rapidly the cosmic ray intensity decreases with depth in the rock:

$$\epsilon = \frac{\Lambda}{\rho}\frac{P}{N} \tag{8.2}$$

8.2 Radionuclides

Let us now move on to a cosmogenic radionuclide in a surface that undergoes no erosion. Initially, the concentration of the nuclide increases almost linearly with time, but after a while, some of these nuclides are lost due to radioactive decay. Eventually, after five or so half lives, a saturation point is reached at which the production rate is balanced by the decay rate. This provides a hard upper limit of the exposure ages that can be measured with cosmogenic radionuclides. The age equation is again a function of P and N, but with the addition of a logarithm and the radioactive decay constant λ:

$$t = -\frac{1}{\lambda}\ln\left(1 - \frac{N\lambda}{P}\right) \tag{8.3}$$

Finally, here is the full ingrowth equation in the general case of a cosmogenic radionuclide with a finite exposure age that also undergoes erosion:

$$N = \frac{P}{\lambda + \rho\epsilon/\Lambda}\left(1 - e^{-(\lambda+\rho\epsilon/\Lambda)t}\right)e^{-\lambda\tau} \tag{8.4}$$

with:

N = concentration (at/g)
P = production rate (at/g/yr)
λ = decay constant (yr^{-1})
Λ = attenuation length (g/cm^{-2})
ρ = density (g/cm^{-3})
ϵ = erosion rate (cm/yr)
t = exposure age (yr)
τ = burial age (yr)

There is one additional parameter, τ, which is the *burial age*, which will be discussed in Section 8.3. The important thing to note here is that there is one equation but three unknowns, the exposure age t, the erosion rate ϵ, and the burial age τ. So in order to solve this equation, two assumptions are needed. For example, if we assume zero burial ($\tau = 0$) and zero erosion ($\epsilon = 0$), then we calculate the exposure age (t). Alternatively, we can assume zero burial and an infinite exposure age ($\tau = 0$, t=∞) and calculate the steady state erosion rate (ϵ). The only way to avoid making such assumptions and simultaneously determining both the erosion rate and the exposure age is to measure two nuclides with different half lives. The most common examples of such paired measurements are $^{10}Be/^{26}Al$ and $^{10}Be/^{21}Ne$. A convenient method to plot and interpret such datasets is the two nuclide diagram or 'banana plot'.

8.3 The 'Banana Plot'

When we plot the $^{26}Al/^{10}Be$-ratio against the ^{10}Be concentration, we obtain the diagram shown in Figure 8.1. Each part of this diagram has its own applications, which will be briefly summarised next.

First consider a sample that plots on the upper line of the diagram. This is the so-called *zero erosion line*, which groups all samples that

can be used for proper exposure dating. So if a sample plots on this line, we have effectively verified the assumption that $\epsilon = 0$. The most important example of studies which require samples that plot on the zero erosion line are exposure dating studies of glacial retreat. When glacial striations can be observed on rock surfaces, this indicates that erosion has been negligible. All those surfaces should plot on the zero erosion line of the banana plot.

The next line down groups all the samples that are in an erosional steady state and that, in principle have an infinite exposure age ($t = \infty$), which effectively means an exposure age that is greater than five times the half lives of both nuclides. Although erosion studies can be performed in bedrock, they are actually most commonly done on sediments. The motivation for this is as follows. Consider a landscape that is in an erosional steady state and that is irradiated by cosmic rays. Cosmogenic nuclides such as ^{10}Be accumulate in the first 2m or so below the surface. These rocks are removed and transported down the drainage network, carrying the cosmogenic nuclide signal with them. By measuring the ^{10}Be content of a single sample of river sediment, the average erosion rate of the entire catchment can be calculated.

So the upper line of the ^{10}Be/^{26}Al banana plot is the zero erosion line, the lower line is the steady state erosion line, and the area between them is called the *steady state erosion island* (or *banana*). Above the erosion island is the 'forbidden zone' of physically impossible cosmogenic nuclide compositions. Samples plotting in this area are likely to suffer from methodological or analytical errors. The large area below the erosion island is the zone of *complex exposure histories*, in which we can find samples that have undergone at least one phase of burial. For example, consider a river sediment derived from a catchment that is in an erosional steady state (e.g., $\epsilon = 0.1$cm/kyr) and has accumulated a measurable amount of cosmogenic ^{10}Be and ^{26}Al. Suppose that this sediment is washed into a cave. The roof of the cave will shield the sample from cosmic rays, so that the production of ^{10}Be and ^{26}Al stops, but their radioactive decay continues. So with time, the sample will move down a line on the banana plot. The burial age can be calculated from the distance of the sample below the steady state erosion island. Obviously, the most common application of burial dating is the dating of cave sediments. By measuring the age of different cave levels in the walls of a river canyon, it is possible to determine the rate of canyon

incision.

8.4 Scaling models

So far in this Chapter, we have assumed that the cosmogenic nuclide production rate P is known. In reality, however, this is only the case for a handful of locations ('calibration sites') in the world, where the exposure history of rocks is known through independent means (e.g. by ^{14}C dating of organic matter or $^{40}Ar/^{39}Ar$ dating of lava flows. These production rates are only valid for the specific conditions (latitude, elevation, age) of each particular calibration site. To apply the cosmogenic nuclide method to other field settings, the production rates must be scaled to a common reference at sea level and high latitude (SLHL). Up to 20% uncertainty is associated with this scaling, constituting the bulk of cosmogenic nuclide age uncertainty.

Although several efforts have been made to directly measure production rate scaling with latitude and elevation using artificial H_2O and SiO_2 targets, all currently used scaling models are based on neutron monitor surveys. The oldest and still most widely used scaling model is that of Lal (1991). This model is a simple set of polynomial equations giving the (spallogenic + muogenic) production rate relative to SLHL as a function of geographic latitude and elevation.

Despite their limitations, the production rate scaling factors allow the calculation of TCN production rates at any location on the Earths surface, assuming that the sample is a slab of zero thickness taken from a horizontal planar surface. If these assumption are not fulfilled, the SLHL production rates must be multiplied by a second set of correction factors, quantifying the extent to which the cosmic rays were blocked by topographic obstructions, snow cover, and the thickness of the sample ('self shielding').

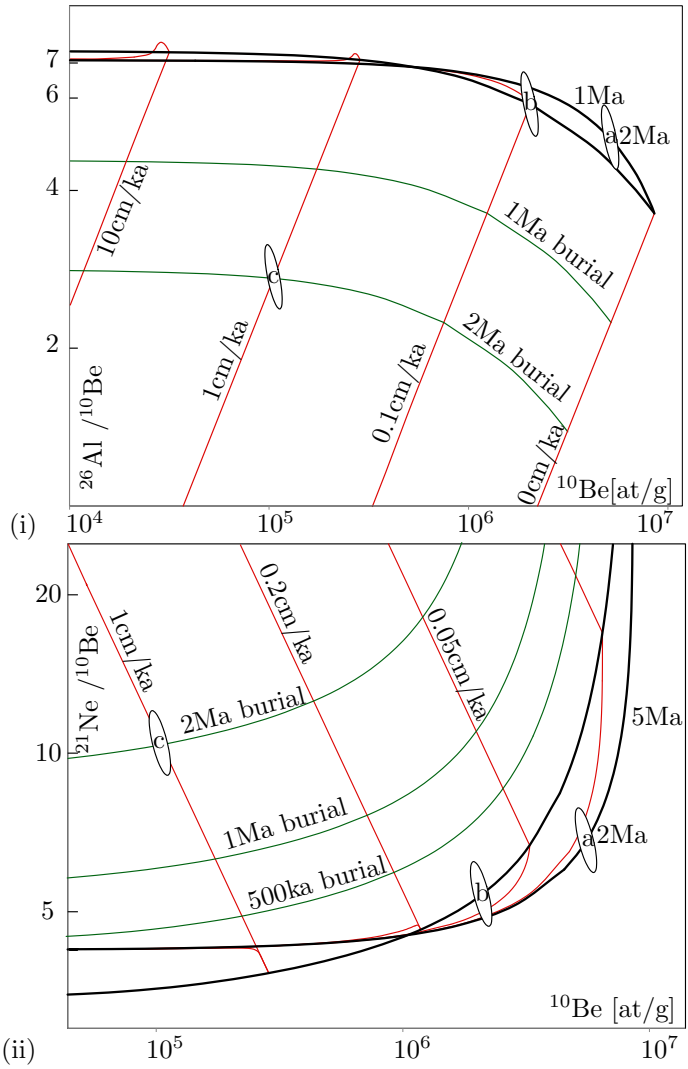

Figure 8.1: ^{10}Be/^{26}Al (i) and ^{21}Ne/^{10}Be (ii) two nuclide ('banana') plots. Sample a has undergone a simple exposure history with t = 2Ma, $\epsilon = 0$ and $\tau = 0$, sample b has undergone steady-state erosion at ϵ = 0.1cm/kyr (t = ∞ and $\tau = 0$), whereas sample c has experience a complex exposure history. Assuming steady-state erosion prior to burial, the data are compatible with ϵ = 1 cm/kyr followed by 2 Myr of burial. The ellipses mark the 95% confidence bounds for the analytical uncertainties (see Section 10).

Chapter 9

U-series disequilibrium methods

In Section 2.4, we saw that the ^{235}U-^{207}Pb and ^{238}U-^{206}Pb decay series generally reach a state of *secular equilibrium*, in which the activity (expressed in decay events per unit time) of each intermediate daughter product is the same, so that:

$$N_{D_n}\lambda_n = \cdots = N_{D_2}\lambda_2 = N_{D_1}\lambda_1 = N_P\lambda_P$$

as described by Equation 2.20. However, certain natural processes can disturb this equilibrium situation, such as chemical weathering, precipitation from a solution, (re-)crystallisation etc. The leads to two new types of chronometric systems:

1. An intermediate daughter isotope in the decay series is separated from its parent nuclide incorporated into a rock or sediment, and decays according to its own half life.

2. A parent nuclide has separated itself from its previous decay products and it takes some time for secular equilibrium to be re-established.

This idea is most frequently applied to the ^{238}U-decay series, notably ^{230}Th and ^{234}U. The first type of disequilibrium dating forms the basis of the ^{234}U-^{238}U and ^{230}Th methods (Sections 9.1 and 9.2). The second forms the basis of the ^{230}Th-^{238}U method (Section 9.3)

9.1 The ^{234}U-^{238}U method

The activity ratio of ^{238}U to its third radioactive daughter ^{234}U in the world's oceans is $A(^{234}U)/A(^{238}U) \equiv \gamma_\circ \approx 1.15$. The slight enrichment of the ^{234}U over ^{238}U is attributed to α-recoil of its immediate parent ^{234}Th and the fact that ^{234}U is more 'loosely bound' inside the crystal lattice of the host mineral, because it is preferentially seated in sites which have undergone radiation damage. Once the oceanic U is incorporated into the crystal structure of marine carbonates, the radioactive equilibrium gradually restores itself with time. The total activity of ^{234}U is made up of a component which is supported by secular equilibrium (and equals the activity of ^{238}U) and an 'excess' component, which decays with time:

$$A(^{234}U) = A(^{238}U) + A(^{234}U)^x_\circ e^{-\lambda_{234}t} \tag{9.1}$$

where $A(^{234}U)^x_\circ$ is the initial amount of excess ^{234}U and $\lambda_{234} = 2.8234 \times 10^{-6}$ yr^{-1} ($t_{1/2} = 245.5$ kyr). Let $A(^{234}U)_\circ$ be the initial total ^{234}U activity. Then:

$$A(^{234}U) = A(^{238}U) + \left[A(^{234}U)_\circ - A(^{238}U)\right] e^{-\lambda_{234}t} \tag{9.2}$$

Dividing by A(^{238}U):

$$\frac{A(^{234}U)}{A(^{238}U)} = 1 + [\gamma_\circ - 1]e^{-\lambda_{234}t} \tag{9.3}$$

Which can be solved for t until about 1 Ma.

9.2 The ^{230}Th method

U and Th are strongly incompatible elements. This causes chemical fractionation and disturbs the secular equilibrium of the ^{238}U decay series in young volcanic rocks. It is commonly found that the activity ratio $A(^{230}Th)/A(^{238}U) > 1$. As expected, the secular equilibrium between ^{234}U and ^{238}U is not disturbed by chemical fractionation, so that $A(^{234}U)/A(^{238}U) = 1$. The total ^{230}Th activity is given by:

$$A(^{230}Th) = A(^{230}Th)^x_\circ e^{-\lambda_{230}t} + A(^{238}U)(1 - e^{-\lambda_{230}t}) \tag{9.4}$$

where $A(^{230}Th)^x_\circ$ is the initial amount of 'excess' ^{230}Th at the time of crystallisation and $A(^{238}U) = A(^{234}U)$ due to secular equilibrium

of the U isotopes. Thus, the first term of Equation 9.4 increases with time from 0 to A(^{238}U) while the second term decreases from $A(^{230}Th)^x_\circ$ to 0. Dividing by $A(^{232}Th)$ yields a linear relationship between $A(^{230}Th)/A(^{232}Th)$ and $A(^{238}U)/A(^{232}Th)$:

$$\frac{A(^{230}Th)}{A(^{232}Th)} = \frac{A(^{230}Th)^x_\circ}{A(^{232}Th)} e^{-\lambda_{230}t} + \frac{A(^{238}U)}{A(^{232}Th)}(1 - e^{-\lambda_{230}t}) \qquad (9.5)$$

This forms an isochron with slope $(1 - e^{-\lambda_{230}t})$, from which the age t can be calculated. This method is applicable to volcanic rocks and pelitic ocean sediments ranging from 3ka to 1Ma.

9.3 The ^{230}Th-^{238}U method

Uranium is significantly more soluble in water than Th. As a result, the intermediate daughter ^{230}Th is largely absent from sea water. Thus, lacustrine and marine carbonate rocks contain some U but virtually no Th at the time of formation. The ^{230}Th activity increases steadily with time as a result of ^{234}U decay. The total ^{230}Th activity consists of a growing component $A(^{230}Th)^s$ that is in secular equilibrium with ^{238}U and a shrinking component $A(^{230}Th)^x$ of 'excess' ^{230}Th produced by the surplus of ^{234}U commonly found in ocean water (see section 9.1):

$$A(^{230}Th) = A(^{230}Th)^s + A(^{230}Th)^x \qquad (9.6)$$

$$\text{with: } A(^{230}Th)^s = A(^{238}U)(1 - e^{-\lambda_{230}t}) \qquad (9.7)$$

$$\text{and: } A(^{230}Th)^x = \frac{\lambda_{230}}{\lambda_{230} - \lambda_{234}} A(^{234}U)^x_\circ \left(e^{-\lambda_{234}t} - e^{-\lambda_{230}t}\right) \qquad (9.8)$$

In which the expression for $A(^{230}Th)^x$ follows from Equation 2.14 and $A(^{234}U)^x_\circ$ denotes the initial amount of excess ^{234}U activity (as in Section 9.1). Taking into account that $A(^{234}U)^x_\circ = A(^{234}U)_\circ - A(^{238}U)$, and dividing by $A(^{238}U)$, we obtain:

$$\frac{A(^{230}Th)^x}{A(^{238}U)} = \frac{\lambda_{230}}{\lambda_{230} - \lambda_{234}} (\gamma_\circ - 1) \left(e^{-\lambda_{234}t} - e^{-\lambda_{230}t}\right) \qquad (9.9)$$

in which $\gamma_\circ \equiv A(^{234}U)/A(^{238}U)$ as defined in Section 9.1. The formation age of the carbonate can be calculated by substituting Equations 9.7 and 9.9 into 9.6 and solving for t.

$$\frac{A(^{230}Th)}{A(^{238}U)} = 1 - e^{-\lambda_{230}t} + \frac{\lambda_{230}}{\lambda_{230} - \lambda_{234}}(\gamma_\circ - 1)\left(e^{-\lambda_{234}t} - e^{-\lambda_{230}t}\right) \quad (9.10)$$

If $\gamma_\circ = 1$ (i.e., the water is in secular equilibrium for U), then Equation 9.6 simplifies to:

$$\frac{A(^{230}Th)}{A(^{238}U)} = 1 - e^{-\lambda_{230}t} \quad (9.11)$$

If $\gamma_\circ \neq 0$, Equation 9.11 yields ages that are systematically too old, unless $t < 100$ka and $\gamma_\circ \leq 1.15$.

Chapter 10

Error propagation

All the methods and equations presented thus far have assumed that all parameters are either known or measured with infinite precision. In reality, however, the analytical equipment used to measure isotopic compositions, elemental concentrations and radioactive half-lives is not perfect. It is crucially important that we quantify the resulting analytical uncertainty before we can reliably interpret the resulting ages.

For example, suppose that the extinction of the dinosaurs has been dated at 65 Ma in one field location, and a meteorite impact has been dated at 64 Ma elsewhere. These two numbers are effectively meaningless in the absence of an estimate of precision. Taken at face value, the dates imply that the meteorite impact took place 1 million years after the mass extinction, which rules out a causal relationship between the two events. If, however, the analytical uncertainty is significantly greater than 1 Myr (e.g. 64 ± 2 Ma and 65 ± 2 Ma), then such of a causal relationship remains very plausible.

10.1 Some basic definitions

Suppose that our geochronological age (t) is calculated as a function (f) of some measurements (X and Y):

$$t = f(X, Y) \tag{10.1}$$

Suppose that we have performed a large number (n) of replicate

measurements of X and Y:

$$\begin{cases} X = & \{X_1, X_2, \cdots, X_i, \cdots, X_n\} \\ Y = & \{Y_1, Y_2, \cdots, Y_i, \cdots, Y_n\} \end{cases} \tag{10.2}$$

It is useful to define the following *summary statistics*:

1. The mean:

$$\begin{cases} \overline{X} \equiv & \frac{1}{n}\sum_{i=1}^{n} X_i \\ \overline{Y} \equiv & \frac{1}{n}\sum_{i=1}^{n} Y_i \end{cases} \tag{10.3}$$

   is a useful definition for the 'most representative' value of X and Y, which can be plugged into Equation 10.1 to calculate the 'most representative' age.

2. The variance:

$$\begin{cases} \sigma_X^2 \equiv & \frac{1}{n-1}\sum_{i=1}^{n}(X_i - \overline{X})^2 \\ \sigma_Y^2 \equiv & \frac{1}{n-1}\sum_{i=1}^{n}(Y_i - \overline{Y})^2 \end{cases} \tag{10.4}$$

   with σ_X and σ_Y the 'standard deviations', is used to quantify the amount of dispersion around the mean.

3. The covariance:

$$cov(X,Y) \equiv \frac{1}{n-1}\sum_{i=1}^{n}(X_i - \overline{X})(Y_i - \overline{Y}) \tag{10.5}$$

   quantifies the degree of correlation between variables X and Y.

$\overline{X}$, $\overline{Y}$, σ_X^2, σ_Y^2 and $cov(X,Y)$ can all be estimated from the input data (X,Y). These values can then be used to infer σ_t^2, the variance of the calculated age t, a process that is known as 'error propagation'. To this end, recall the definition of the variance (Equation 10.4):

$$\sigma_t^2 \equiv \frac{1}{n-1}\sum_{i=1}^{n}(t_i - \overline{t})^2 \tag{10.6}$$

We can estimate $(t_i - \overline{t})$ by differentiating Equation 10.1:

$$t_i - \overline{t} = (X_i - \overline{X})\frac{\partial f}{\partial X} + (Y_i - \overline{Y})\frac{\partial f}{\partial Y} \tag{10.7}$$

Plugging Equation 10.7 into 10.6, we obtain:

$$\sigma_t^2 = \frac{1}{n-1}\sum_{i=1}^{n}\left[(X_i - \overline{X})\left(\frac{\partial f}{\partial X}\right) + (Y_i - \overline{Y})\left(\frac{\partial f}{\partial Y}\right)\right]^2 \tag{10.8}$$

$$= \sigma_X^2\left(\frac{\partial f}{\partial X}\right)^2 + \sigma_Y^2\left(\frac{\partial f}{\partial Y}\right)^2 + 2\ cov(X,Y)\frac{\partial f}{\partial X}\frac{\partial f}{\partial Y} \tag{10.9}$$

This is the general equation for the propagation of uncertainty with two variables, which is most easily extended to more than two variables by reformulating Equation 10.9 into a matrix form:

$$\sigma_t^2 = \begin{bmatrix} \frac{\partial t}{\partial X} & \frac{\partial t}{\partial Y} \end{bmatrix} \begin{bmatrix} \sigma_X^2 & cov(X,Y) \\ cov(X,Y) & \sigma_Y^2 \end{bmatrix} \begin{bmatrix} \frac{\partial t}{\partial X} \\ \frac{\partial t}{\partial Y} \end{bmatrix} \tag{10.10}$$

where the innermost matrix is known as the *variance-covariance* matrix and the outermost matrix (and its transpose) as the *Jacobian matrix*. Let us now apply this equation to some simple functions.

10.2 Examples

1. addition:

$$t = aX + bY \Rightarrow \frac{\partial t}{\partial X} = a, \frac{\partial t}{\partial Y} = b \tag{10.11}$$

$$\Rightarrow \sigma_t^2 = a^2\sigma_X^2 + b^2\sigma_Y^2 + 2ab\ cov(X,Y) \tag{10.12}$$

2. subtraction:

$$t = aX - bY \Rightarrow \cdots \Rightarrow \sigma_t^2 = a^2\sigma_X^2 + b^2\sigma_Y^2 - 2ab\ cov(X,Y) \tag{10.13}$$

3. multiplication:

$$t = aXY \Rightarrow \frac{\partial t}{\partial X} = aY, \frac{\partial t}{\partial Y} = aX \tag{10.14}$$

$$\Rightarrow \sigma_t^2 = (aY)^2\sigma_X^2 + (aX)^2\sigma_Y^2 + 2a^2XY\ cov(X,Y) \tag{10.15}$$

$$\Rightarrow \left(\frac{\sigma_t}{t}\right)^2 = \left(\frac{\sigma_X}{X}\right)^2 + \left(\frac{\sigma_Y}{Y}\right)^2 + 2\frac{cov(X,Y)}{XY} \tag{10.16}$$

4. division:

$$t = a\frac{X}{Y} \Rightarrow \cdots \Rightarrow \left(\frac{\sigma_t}{t}\right)^2 = \left(\frac{\sigma_X}{X}\right)^2 + \left(\frac{\sigma_Y}{Y}\right)^2 - 2\frac{cov(X,Y)}{XY} \tag{10.17}$$

5. exponentiation:

$$t = a\ e^{bX} \Rightarrow \frac{\partial f}{\partial X} = ab\ e^{bX} \Rightarrow \sigma_t^2 = (bt)^2 \sigma_X^2 \tag{10.18}$$

6. logarithms:

$$t = a\ \ln(bX) \rightarrow \frac{\partial f}{\partial X} = \frac{a}{X} \Rightarrow \sigma_t^2 = \left(\frac{a}{X}\right)^2 \sigma_X^2 \tag{10.19}$$

10.3 Accuracy vs. precision

Recall the definition of the arithmetic mean (Equation 10.3):

$$\overline{X} \equiv \frac{1}{n} \sum_{i=1}^{n} X_i$$

Applying the equation for the error propagation of a sum (Equation 10.12):

$$\sigma_{\overline{X}}^2 = \frac{1}{n} \sum_{i=1}^{n} \sigma_{X_i}^2 = \frac{\sigma_X^2}{n} \tag{10.20}$$

where we assume that all n measurements were done *independently*, so that $cov(X_i, X_j) = 0\ \forall$ i, j. The standard deviation of the mean is known as the standard error:

$$\sigma_{\overline{X}} = \frac{\sigma_X}{\sqrt{n}} \tag{10.21}$$

This means that the standard error of the mean monotonically decreases with the square root of sample size. In other words, we can arbitrarily increase the *precision* of our analytical data by acquiring more data. However, it is important to note that the same is generaly not the case for the *accuracy* of those data. The difference between precision and accuracy is best explained by a darts board analogy:

Whereas the analytical precision can be computed from the data using the error propagation formulas introduced above, the only way to get a grip on the accuracy is by analysing another sample of independently determined age. Such test samples are also known as 'secondary standards'.

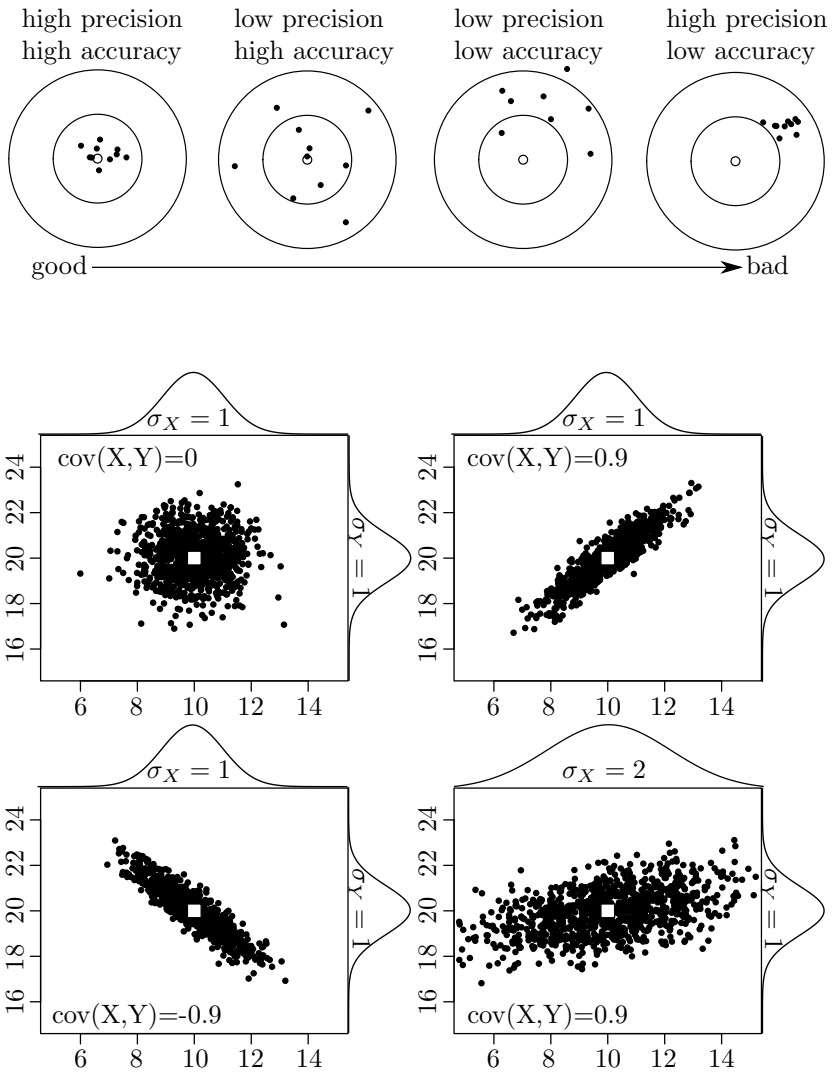

Figure 10.1: Four datasets of 100 random numbers (black dots) which have the same means (white squares) but different (co-)variance structures. The marginal distributions of the X and Y variables are shown as 'bell curves' on the top and right axis of each plot.

Chapter 11

Exercises

1. If helium ions (mass number = 4) are accelerated with a voltage of 10 kV in a mass spectrometer, at what speed are they emitted from the source? Recall that 1 atomic mass unit (amu) = 1.66×10^{-27} kg and the elementary charge is 1.602×10^{-19} C. [Answer: 695 km/s]

2. We are trying to estimate the Rb concentration in a rock for the purpose of whole rock Rb-Sr dating. To this end, we use a spike with a Rb concentration of 7.5 ppm containing 99.4% ^{87}Rb and 0.6% ^{85}Rb (these are atomic abundances). We mix 3.5g of the spike with 0.25g of sample dissolved in 50g. The ^{87}Rb/^{85}Rb-ratio of the mixture is 1.55, as measured by mass spectrometry. What is the Rb concentration in ppm? Note that natural Rb comprises of 27.825% ^{87}Rb and 72.165% ^{85}Rb. [Answer: 120 ppm]

3. A biotite contains 465ppm Rb and 30ppm Sr with a ^{87}Sr/^{86}Sr-ratio of 2.50. Given an initial ^{87}Sr/^{86}Sr-ratio of 0.7035, what is the age of the biotite? Natural Rb has an atomic mass of 85.4678 and comprises 72.165% ^{85}Rb and 27.825% ^{87}Rb, which has a half life of $t_{1/2} = 48.8$ Gyr. Sr has an atomic mass of 87.62. Its non-radiogenic isotopes occur with the following abundances: ^{84}Sr/^{86}Sr = 0.056584 and ^{86}Sr/^{88}Sr = 0.1194. [Answer: 2.36 Ga]

4. What is the U-Th-Pb age of a zircon with the following composition: U = 792.1 ppm, Th = 318.6 ppm, Pb = 208.2 ppm. Atomic masses for U, Th and Pb in the zircon are 238.04, 232.04 and

205.94, respectively. The isotopic composition of the Pb is as follows: ^{204}Pb = 0.048%, ^{206}Pb = 80.33%, ^{207}Pb = 9.00%, ^{208}Pb = 10.63%. Assume the following initial Pb composition: 204 : 206 : 207 : 208 = 1.00 : 16.25 : 15.51 : 35.73. The decay constants for ^{238}U, ^{235}U and ^{232}Th are given in Section 5. ^{238}U/^{235}U = 137.88. Calculate the ^{206}Pb/^{238}U, ^{207}Pb/^{235}U, ^{208}Pb/^{232}Th and ^{206}Pb/^{207}Pb-age of the zircon. Give an account of its formation history.
[Answer: 1.405, 1.523, 1.284 and 1.689 Ga]

5. A biotite was separated from granite and dated with the K-Ar method. The analytical data are as follows: K_2O = 8.45 weight %, radiogenic ^{40}Ar = 6.015×10^{-10} mol/g. What is the K-Ar age of the biotite? The atomic mass of K is 39.098 (and oxygen 15.9994), with an isotopic composition that comprises 93.258% ^{39}K, 6.730% ^{41}K and 0.01167% ^{40}K, which has a half-life of $t_{1/2}$ = 1.248 Gyr. Recall that only 10.72% of the ^{40}K decays to ^{40}Ar, with the remaining 89.28% turning into ^{40}Ca. [Answer: 47.7 Ma]

6. Consider a biotite with a conventional K-Ar age of 384Ma. A ^{40}Ar/^{39}Ar step-heating experiment yields the following data:

% ^{39}Ar released	7	15	20	25	35	70	100
^{40}Ar*/^{39}Ar	2.27	4.97	6.68	9.58	10.25	10.10	10.26

The analysis was done using a co-irradated 1.062 Ga biotite age standard yielding a ^{40}Ar*/^{39}Ar-ratio of 27.64. Construct the ^{40}Ar/^{39}Ar age spectrum and use this to comment on the thermal history of the host rock. $t_{1/2}(^{40}\text{Ar})$ = 1.248 Gyr.
[Answer: 115, 243, 319, 442, 470, 463 and 470 Ma]

7. How many cm^3 of helium does a rock weighing 1 kg and containing 2 ppm of uranium produce after 1 billion years? The molar volume of an ideal gas is 22.414 litres. Uranium has an atomic mass of 238.04 with ^{238}U/^{235}U = 137.88. Decay constants of U are given in Section 5. [Answer: 0.27 cm^3]

8. Repeated analysis of the Fish Canyon zircon age standard (t=27.8 Ma) yields the following fission track data:

Compute the average ζ-calibration factor and use this to calculate the zircon fission track ages of the following rocks:

ρ_s ($\times 10^5 \mathrm{cm}^{-2}$)	ρ_i ($\times 10^6 \mathrm{cm}^{-2}$)	ρ_d ($\times 10^5 \mathrm{cm}^{-2}$)
36.56	6.282	2.829
38.97	7.413	3.313
56.53	7.878	2.457
41.05	8.578	3.485
45.87	6.985	2.482

	ρ_s ($\times 10^5 \mathrm{cm}^{-2}$)	ρ_i ($\times 10^6 \mathrm{cm}^{-2}$)	ρ_d ($\times 10^5 \mathrm{cm}^{-2}$)
Tardree rhyolite	60.49	2.66	1.519
Bishop tuff	6.248	1.299	0.081

The half-life of ^{238}U is $t_{1/2} = 4.47$ Gyr.
[Answer: Tardree – 57 Ma; Bishop – 643 ka]

9. The Dry Valleys of Antarctica represent one of the oldest landscapes in the world, with erosion rates as low as 2.5 cm/Myr. Cosmogenic ^{21}Ne and ^{10}Be accumulate in quartz at SLHL production rates of 20 at/g/yr and 4.5 at/g/yr, respectively. What is the expected ^{21}Ne/^{10}Be-ratio in these surface rocks? The rock density is 2.65 g/cm^3 and the half-life of ^{10}Be is 1.36 Myr. The attenuation length for cosmic ray neutrons is Λ=160 g/cm^{-2}. [Answer: 59.1]

10. A fossil mollusc has been found in a Quaternary beach formation and its activity ratio measured as A(^{230}Th) / A(^{238}U) = 0.6782. Determine the age of the fossil assuming that $\gamma_\circ = 1.15$ and given that the half lives of ^{230}Th and ^{234}U are 75,380 and 245,500 years, respectively. [Answer: 100kyr]

Chapter 12

Matlab practicals

Matlab is a mathematical scripting language that is both powerful and easy to use. The full version of the software is very expensive but a reasonably complete student version can be purchased for £55 + VAT from http://mathworks.com. Alternatively, Octave is an open source clone of Matlab that can be downloaded for free from http://www.gnu.org/software/octave.

12.1 Introduction to Matlab

This exercise will present a brief tutorial of the most basic functionality in Matlab, which will cover most commands you will need for the subsequent computer practicals.

```
% Anything following a percent symbol is a
% comment and is ignored by Matlab. It is
% considered good practice to document your
% code with lots of comments, as will be
% done for this tutorial.

% Ending a line with a semi-colon
% suppresses output to the console:
'be loud'
'stay quiet';

% Matlab can be used as a fancy calculator:
```

```
1 + 1
sqrt(2)
exp(log(10))

% Intermediate values can be stored in variables:
foo = 2;
bar = 4;
foo = foo*bar;
foo

% Data can be entered as vectors:
x = [0 2 4 6 8 10]
% or using shorthand syntax:
y = 0:2:10

% Define a matrix
z = [1 2 3
     4 5 6
     7 8 9];

% Accessing one or more elements
% from a matrix or vector:
x(3)
y(1:3)
z(1:2,2:3)

% Attention: '*', '/' and '^' symbols
% are reserved for matrix operations:
a = [1 1 1]  % row vector
b = [1;1;1]  % column vector
a*b

% Use '.*', './' and '.^' for
% element-wise operations:
a.*a

% Transpose of a matrix:
z'

% In addition to Matlab's built-in operators
```

```
% and functions, you can also define your own:
function out = cube(in)
  out = in^3;
end

% After saving the code in a file named cube.m,
% you can then use this function as follows:
c3 = cube(3)

% A useful feature of Matlab that is missing from
% most other programming languages is the ability
% to accommodate several output parameters:
function [m,s] = basicStats(dat)
  m = mean(dat); % mean
  s = std(dat);  % standard deviation
end

% create a row vector of 10 random numbers
randnum = rand(1,10);
% use our new function
[m,s] = basicStats(randnum)

% Conditional statement:
function coinToss
  % 'rand' produces numbers between 0 and 1
  if (rand > 0.5)
    % display a message to the console
    disp('head')
  else
    disp('tail')
  end
end

% For loop:
for i=1:10,
  coinToss
end

% List all the variables in the current workspace:
who
```

```
whos

% Remove some or all variables
% from the current workspace:
clear m,s
who
clear all
who

% Copy the 'coinToss' function into a text file
% named 'coinToss.m' and save it in the current
% directory. You can then load the contents of
% the file by simply typing its name without
% the '.m' extension:
coinToss

% Basic file management is done with UNIX commands:
pwd   % pass the working directory
cd .. % move up one directory
ls    % list all files in the current directory

% Use the above commands to navigate to the
% directory containing the 'population.csv' file.
% To view the contents of the file:
type('population.csv')

% To read the actual population dataset
% into memory, ignoring the header:
pop = csvread('population.csv',1,0);

% To access the help files of the 'csvread'
% function and find out the meaning of the
% various input arguments:
doc csvread

% Incidentally, the 'type' function can also
% be used to view the Matlab code of built-in
% and other functions:
type('mean')
```

```
% Plot the first column of 'pop'
% against the second one:
plot(pop(:,1),pop(:,2),'-k')
title("World population through time")
xlabel('year')
ylabel('population [millions]')

% Get the number of rows and columns of the dataset:
[nc,nr] = size(pop);

% Extract the data from 1965 until 2014:
years = pop(:,1);
pop65 = pop(years>=1965,:);

% Fit a linear model through these data:
x = pop65(:,1);
y = pop65(:,2);
[fit,S] = polyfit(x,y,1);
% We won't use S today but we will in Practical 4!

% Create a new figure window
figure(2)
plot(x,y,'ok')
hold on
ypred = fit(1)*x+fit(2);
plot(x,ypred,'-k')

% Close all plot windows:
close all;
```

And that concludes this short tutorial. Now try to calculate a Rb-Sr age by regressing an isochron through the following data (recall that $\lambda_{87} = 0.0000142$ Myr^{-1}.

$^{87}Sr/^{86}Sr$	0.707	0.736	0.771	0.757	0.785
$^{87}Rb/^{86}Sr$	1.00	5.00	10.00	8.00	12.00

12.2 U-Th-Pb data reduction

You are supplied with two data files that were produced by the quadrupole laser ablation ICP-MS system at UCL's London Geochronology Centre. At the time of the analysis, this instrument could not resolve ^{204}Pb from the isobaric interference at ^{204}Hg. Therefore, it is not possible to apply a common lead correction as explained in Section 5. However, this does not cause any major issues to us because:

1. The mineral analysed is zircon, which is a mineral that incorporates very little common Pb in its crystal structure during crystallisation.

2. The ages are sufficiently old for the radiogenic Pb to dominate the common Pb component by orders of magnitude.

In this exercise, we will use standard-sample bracketing (Section 3.3) to process some raw mass spectrometer data in `Matlab`:

1. Load the input files `91500.csv` (sample) and `GJ1.csv` (standard) into `Matlab`.

2. Plot the ^{238}U signal against time.

3. Given that GJ-1 has a known age of 600.3874 Ma, what are its expected ^{206}Pb/^{238}U, ^{207}Pb/^{235}U and ^{208}Pb/^{232}Th ratios?

4. Compare these values with the measured ratios, computed as the arithmetic mean signal. Is there a significant difference between the measured and the expected ratios? What could be causing this?

5. Calculate a correction factor by dividing the measured GJ-1 ratios by the expected values.

6. Calculate the measured isotopic ratios for sample 91500.

7. Apply the correction factor calculated in step 5 to these measurements.

8. What is the age of 91500?

9. Can you plot the results on a Wetherill concordia diagram?

12.3 $^{40}Ar/^{39}Ar$ data reduction

In this exercise, we will use `Matlab` to reduce some synthetic $^{40}Ar/^{39}Ar$ data. You are provided with three input files:

1. `smpl.csv`: ^{36}Ar, ^{39}Ar and ^{40}Ar as a function of time (t) for the sample.
2. `stnd.csv`: the same data for the standard, which is a Fish Canyon sanidine with a conventional K-Ar age of 27.8 Ma.
3. `blnk.csv`: a 'blank' run, i.e. a measurement of the background levels of Argon present in the mass spectrometer in the absence of a sample.

To perform the data reduction, please follow the following steps:

1. Load the three input files.
2. Plot the ^{40}Ar signal of the sample against time. Do the same for the ^{36}Ar signal in the blank. What's the difference?
3. Perform a linear regression of the ^{36}Ar, ^{39}Ar and ^{40}Ar signals through time and determine the intercept at t=0.
4. Subtract the blank signals from the sample and standard signals.
5. Apply an atmospheric correction assuming that all ^{36}Ar has an atmospheric origin.
6. Calculate the J-value of the standard.
7. Calculate the age of the sample.

12.4 Error propagation

This exercise will build on the results from the previous two practicals.

1. Plot the $^{206}Pb/^{238}U$-ratios of the sample against those of the standard (data from Section 12.2). Verify that the covariance between the two can safely be neglected.
2. Calculate the standard errors of the mean $^{206}Pb/^{238}U$ signal ratios for the sample (91500) and the standard (GJ-1), using `Matlab`'s `mean` and `std` functions.

3. Propagate the analytical uncertainties of the U-Pb age, ignoring the covariance terms. Recall that

$$t = \frac{1}{\lambda_{238}} \ln\left(1 + \frac{^{206}Pb}{^{238}U}\right)$$

If you want you can use the simplifying approximation that ln(1+X) $\approx X$ if X $\ll$ 1 (this assumption may not be correct for the ^{207}Pb/^{235}U-age).

4. Compute the analytical uncertainties associated with the linear extrapolation of the argon signals of the sample and the standard in Section 12.3. All the relevant information is provided in the output of the `polyfit` function:

```
help(polyfit)
...
[P,S] = POLYFIT(X,Y,N) returns the polynomial
coefficients P and a structure S for use with
POLYVAL to obtain error estimates for predictions.
S contains fields for the triangular factor (R)
from a QR decomposition of the Vandermonde matrix
of X, the degrees of freedom (df), and the norm
of the residuals (normr). If the data Y are
random, an estimate of the covariance matrix
of P is (Rinv*Rinv')*normr^2/df, where Rinv
is the inverse of R.
```

Based on these instructions, I have written the following function to calculate the standard errors of the fitting parameters from the second output parameter of the `polyfit` function:

```
function se = S2se(S)
  covmat = (inv(S.R)*inv(S.R'))*S.normr^2/S.df;
  se = sqrt(diag(covmat));
end
```

5. Use these error estimates to propagate the analytical uncertainty of the J-value and the sample age. Again you can use the linear approximation to the age equation mentioned in point 3.

12.5 Fission tracks

In this exercise, you will use your `Matlab` programming skills to calculate some fission track ages. You are given the following datasets:

1. `DUR.csv`: a table with two columns listing the number of spontaneous tracks N_s and induced tracks N_i counted in 25 grains of an apatite age standard (t = 31.4 Ma) from Durango, Mexico. Note that these pairs of tracks were counted over the same area, so that $\rho_s/\rho_i = N_s/N_i$ in Equation 7.9.

2. `MD.csv`: a similar table for an apatite sample from Mount Dromedary, Australia.

You will need to:

1. Rewrite Equation 7.9 in terms of the ζ calibration factor and use this new formula to calculate the ζ factor for each single grain analysis of the Durango age standard. Use a dosimeter track density of $\rho_D = 300,000$ cm^{-2}.

2. Use the mean of these ζ factors to calculate the age of the Mount Dromedary sample (i.e., the single grain ages and their mean).

3. Propagate the analytical uncertainties for each of those single grain ages, using the fact that fission track counts (N, say) follow a Poisson distribution for which it is true that:

$$\sigma_N^2 = N$$

   To simplify the calculations, you can also use the following approximation:

$$\frac{1}{\lambda}\ln\left(1+\frac{g_i}{g_s}\lambda\zeta\rho_d\frac{N_s}{N_i}\right) \approx \frac{g_i}{g_s}\zeta\rho_d\frac{N_s}{N_i}$$

4. How does the single grain age precision of the fission track method compare to the U-Pb and ^{40}Ar/^{39}Ar age uncertainties in Sections 12.2 and 12.3? Also compare with the standard deviation and standard error of the mean age of Mount Dromedary apatite.